

Self-Supervised Learning for Point Clouds Data: A Survey

Changyu Zeng, Wei Wang, Anh Nguyen, Yutao Yue*

arXiv:2305.11881v1 [cs.CV] 9 May 2023

Abstract—The 3D point cloud is a crucial type of data collected by LiDAR sensors and widely used in transportation-related fields due to its concise description and accurate localization. To better capture the hierarchical representation of the point cloud, deep neural networks (DNNs) are employed to process considerable disorder 3D points and accomplish promising achievements in various computer vision tasks such as pedestrian detection and vehicle recognition. However, point cloud labeling is time-consuming and labor-intensive due to the disordered and sparse attribute of the point cloud. Therefore, self-supervised learning (SSL), an unsupervised training paradigm that mines effective information from the data itself without human annotations, is considered an essential solution for moving away from label dependency via its brilliant pre-training task design. This paper provides a comprehensive survey of recent advances in deep neural network-based point cloud SSL. We initially introduce the definition, motivation, general pipeline as well as background to describe the concept of SSL and its combination with point cloud in detail. In addition, we present an innovative taxonomy of point cloud SSL methods, separating current approaches into four broad categories based on the pretexts' characteristics. We then summarize and compare the performances of the proposed SSL methods in literature on multiple downstream tasks quantitatively and qualitatively on benchmark datasets. Finally, feasible future research directions are provided to alleviate current limitations of point cloud SSL and also enhance feature extraction capability and generalizability of pre-training models.

Index Terms—Self-Supervised Learning, Point Clouds, Representation Learning, Pretext Task, Transfer Learning

1 INTRODUCTION

With the rapid development of 3D data processing technologies, an increasing number of relevant applications have emerged in both industrial and daily usage, such as indoor

- Changyu Zeng is with the Institute of Deep Perception Technology, JITRI, Wuxi, China; the Department of Computing, School of Advanced Technology, Xi'an Jiaotong-Liverpool University, Suzhou, China; the Department of Computer Science, University of Liverpool, Liverpool, United Kingdom. Email: changyu.zeng17@student.xjtlu.edu.cn
- Wei Wang is with the Department of Computing, School of Advanced Technology, Xi'an Jiaotong-Liverpool University, Suzhou, China. Email: wei.wang03@xjtlu.edu.cn
- Anh Nguyen is with the Department of Computer Science, University of Liverpool, Liverpool, United Kingdom. Email: anh.nguyen@liverpool.ac.uk
- Yutao Yue is with the Institute of Deep Perception Technology, JITRI, Wuxi, China; XJTLU-JITRI Academy of Industrial Technology, Xi'an Jiaotong-Liverpool University, Suzhou, China; Department of Mathematical Sciences, University of Liverpool, UK. Email: yueyutao@idpt.org, *Corresponding author

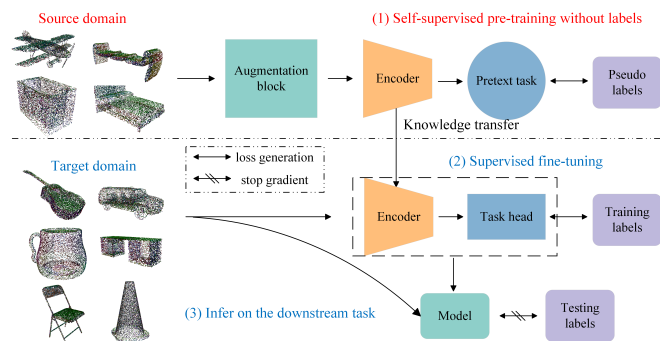


Fig. 1. The general pipeline of SSL used in the point cloud data. (1) Pre-training stage: the point cloud data is first pre-processed through the augmentation block and then fed into the point-specific encoder to capture feature representation. Then the features are utilized to complete a well-design pretext task, where the output will compare with the pseudo label derived by the original data to generate a loss and update encoder parameters via back-propagation. (2) Supervised fine-tuning stage: the well-trained encoder will be transferred to the target domain. A task head will be trained with the training labels in a supervised manner to complete the downstream task. (3) Inference stage: the encoder and task head are concatenated as a model to execute inference in the test set. The effectiveness of the SSL pre-training framework could be evaluated through the performance of the model on the downstream task.

navigation [1], autonomous driving [2], and object modeling [3]. In particular, LiDAR is one of the indispensable sensors to capture disorder 3D point cloud data from complicated traffic scenes, which could be further parsed to achieve challenging tasks like pedestrian detection [4] and road semantic segmentation [5] via combining the strong inference ability of deep neural networks (DNNs).

However, several issues in the current supervised point cloud DNNs hinder their further development. Initially, accurate environment perception via reliable point clouds DNNs requires millions of labeled data as the input source, while point cloud annotating is labor-intensive and time-consuming due to its disordered and sparse nature [6]. Besides, manual labeling will inevitably lead to mistakes such as mislabeling and omission due to the excessive number of labeled points. Another long-standing problem is that the supervised learning paradigm struggles to capture the underlying patterns of new data and fails to generalize the pre-training model to downstream tasks because of overfitting caused by noisy labels [7].

The aforementioned issues motivate research develop-

ment in extracting effective feature representation in the point cloud field via self-supervised learning (SSL) manner to learn the implicit representation embedded in the data without manual labels. Not only does it solve the problem of difficult and expensive labeling, but it also benefits relieving domain adaptation (DA) issues [8] and improves model generalization ability. In the SSL paradigm, basic geometric as well as advanced semantic information can be extracted as knowledge encoded in the form of parameters and migrated to downstream tasks under the transfer learning setup. This progress approximates human learning that discovers objective principles of the world by observing phenomena and summarizing them into a system of experience and knowledge.

Fig. 1 shows the general pre-train pipeline of SSL in point cloud data. Overall, the goal of SSL is to pre-train an encoder on an unlabeled large-scale point cloud dataset (source domain) and transfer the well-trained network to other datasets (target domain) for various downstream tasks. Commonly, the complete SSL framework contains the following modules:

- **Data augmentation:** The raw input point cloud data is augmented into numerous versions through easy-to-implement preprocessed operations such as translation, rotation, flip, and adding noise [9]. The objective is to expand the diversity of the data and provide subjects for subsequent pretext tasks. The details will be discussed in Section 2.4.
- **Encoder:** The encoder is a point-specific network that captures the hierarchical representation of the input point cloud data. In this paper, we will introduce some commonly used point cloud encoders that either learn from downsampling layer-by-layer [10], [11] or focus on the local area to capture the association between blocks [12], [13]. The details will be discussed in Section 2.5.
- **Pretext task:** The core of the whole framework is to design a pretext task that mines the hidden self-supervision signal via the interaction between the encoder and data. This part is the focus of the whole review and will be discussed in detail in Section 3.
- **Knowledge transfer:** The well-trained encoder will be transferred to another dataset with the knowledge gained in the source domain after completing the pretext task. A task head is then constructed and trained by a few labels in the target domain as the supervision signals to fine-tune the whole architecture. The details will be discussed in Section 4.
- **Downstream task:** To evaluate the effectiveness of the SSL framework, the pre-trained encoder will be transferred and evaluated on another dataset for performance tests such as object classification, part segmentation, and object detection. A higher evaluation metric for the downstream task represents a better SSL pre-training effect. The details will be discussed in Section 4.

Thriving progress has been made in the field of point cloud SSL recently. While there is not a systematic survey to summarize such prominent research works except [14], which organized outlining unsupervised point cloud repre-

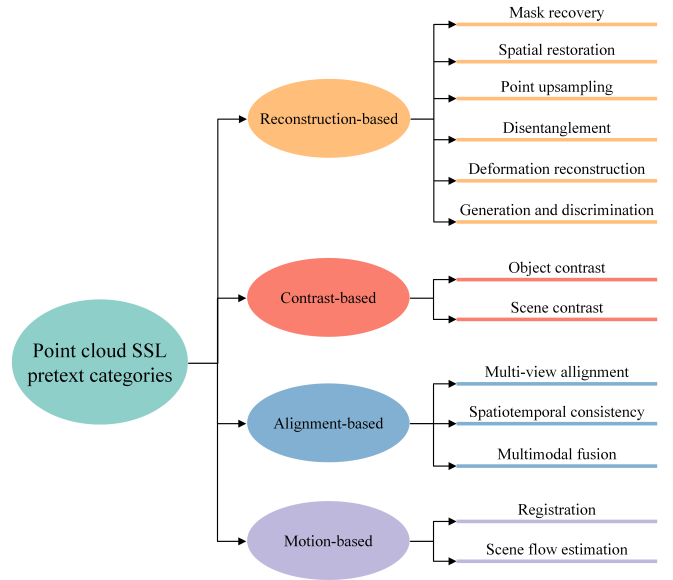


Fig. 2. Taxonomy of SSL pretext tasks for point cloud data. The classification is based on the intersection method between the pretext tasks and the input point cloud data.

sentation learning. However, [14] lacked a summary of the state-of-the-art SSL models as well as a detailed demonstration of rare approaches. Therefore, we were motivated to conclude remarkable SSL work in the point cloud field in the last few years and produce a reviewed paper providing an attentive explanation of each module of the point cloud SSL framework displayed in Fig. 1. Compared with [14], we propose an advanced taxonomy of the SSL pretext tasks shown in Fig. 2, which is more reasonable and methodical to classify the current pretext tasks according to their characteristics. Besides, our paper contains more comprehensive content, for example, the module about point cloud data augmentation, a description of point cloud data properties, and the way different proxy tasks generate pseudo labels. Our contributions can be summarized as follows:

- **Systematic and novel taxonomy:** We propose a novel and systematic taxonomy to formalize the diverse kinds of point cloud SSL methods. This new classification criterion displays our understanding from an advanced perspective and categorizes all current methods into a total of four broad categories. For each broad category, it can be further subdivided into more fine-grained sub-categories according to the variations in feature utilizing aspects as detailed in Fig. 2.
- **Comprehensive and detailed summary:** We conduct a comprehensive review of SSL point cloud methods, including the background of SSL as well as point clouds, commonly used point cloud SSL datasets and models, four types of point cloud SSL pretext tasks, various downstream tasks with performance comparison, and practical future directions. For each section, we explain each conceptual approach clearly using standard academic expressions with images, tables, and formulas.
- **Exhaustive dataset summary and comparison:** We

summarized the unique characteristics of the 18 most frequently utilized datasets in the point cloud field. In addition, we also compared the performance of different SSL point cloud methods on these datasets separately according to various downstream tasks.

- **Feasible future directions:** Based on current research progress, we discuss the present technique limitations and propose potential improvement directions in the point cloud SSL field. These ideas combine the latest thoughts and trends in other fields to make point cloud SSL methods more generalizable and advanced.

The rest of the survey is organized as follows: Section 2 introduces the background of SSL and point cloud data, containing the SSL development history, point cloud properties, point cloud datasets summary, point cloud data augmentations, commonly used point cloud models, pseudo labels, and loss functions. Section 3 demonstrates the proposed taxonomy with exhaustive instances elaboration. Section 4 summarizes the frequently utilized downstream tasks and compares the performance of different SSL methods on these tasks. Section 5 discusses the limitations of current approaches and proposes potential future directions. Finally, Section 6 concludes the whole review.

2 BACKGROUND

2.1 Self-supervised learning in the language and image domain

Before introducing SSL methods in the point cloud field, we will briefly describe the development history of SSL methods in the language and image domains. The purpose is to give readers a general understanding of SSL methods and their core ideas across different domains.

Natural Language Processing (NLP) is where SSL was first developed. After the revolutionary research Word2Vec [15] was released, NLP models began to trend towards label-dependency removal and rapidly progressed leveraging these SSL paradigms across many NLP pretext tasks. Specifically, after converting words into vectors and utilizing the relationship between the representation and context, models could learn semantic representations from neighboring words or sentences through task formulations such as next sentence prediction [16], auto-regressive language modeling [17], or sentence permutation [18], etc. During this exploration, landmark network models such as GPT [17] and BERT [16] were born, and their variants were extended to other fields and achieved promising performance successfully.

In the field of images, SSL algorithms are constantly updated in the design of pretext tasks. From simple tasks like relative position prediction [19], [20] and rotation angle prediction [21], to reconstructing the block being masked by surrounding visible pictures [22], [23], different self-supervised methods impose simple variations on image data and extract features by recovering to the original input. In recent years, the academic community has converged its attention on the paradigm of contrastive learning [24]–[26], which aims to differentiate positive and negative samples by comparison using data augmentation techniques.

Additionally, free semantic label-based [27]–[30] and cross-modal-based methods [31]–[33] have been proposed, which learn significant representations via automatically generated semantic labels and extra information from other modalities, respectively. All aforementioned significant works inspired the development of SSL in the point cloud field. Similar ideas could be transferred from 2D to 3D in the case of adapting for data peculiarities.

Although data types vary from domain to domain, the core idea of SSL remains the same: leverage data characteristics for transformation processing and make transformed data consistent with the original input in terms of feature representation by contrasting or reconstruction.

2.2 Properties of the point cloud data

As mentioned above, data properties are distinct between language, image, and point cloud. In this section, we will focus on describing the unique features that distinguish point cloud data from the other two.

Language is a complex and abstract data type that contains ambiguous information due to its versatility and richness. It is expressed by a sequence of words, which are discrete and unstructured in the representation space [25]. In contrast, images are more intuitive and explicit for human perception. They are 2D data consisting of a matrix of pixel values that represent the color, texture, and shape information of an object in high-dimensional space [34].

Point cloud data is similar to image data in terms of visual format and could be regarded as 3D stereo images with depth information. However, the attributes of point cloud data are completely different in geometric representation. Specifically, a point cloud is a collection of discrete, disordered, and topology-free 3D points. The most basic information contained in the point is the position coordinate (x_i, y_i, z_i) in Euclidean space where i is the number of points in the object. Alternatively, there are also other optional attributes such as color, intensity, reflectivity, etc., specifying the physical properties of the point cloud in more detail. The input order is trivial for point cloud data and will not affect semantic meaning while it is crucial for images and language where various words or pixel sequences lead to totally divergent connotations. Additionally, point cloud data is invariant to rigid transformation which means that it remains unchanged after rotation and translation. Such exclusive properties could be summarized as follows:

- **Sparsity:** The point cloud data is discretely distributed on the surface of the scanned object or scene.
- **Non-uniformity:** The distance between points is not fixed and is determined by various factors such as the instrument’s sampling strategy, relative position, and scanning range.
- **Incomplete data:** Some parts of real-scanned surfaces are incomplete due to self or external occlusion.
- **Data noise:** It is inevitable that noise from environmental factors or inaccuracies in instruments will be present.
- **Permutation invariance:** The order of points does not affect the overall semantic representation of point cloud objects, so identical point cloud objects can be expressed by various matrices.

TABLE 1

Summary of commonly used point cloud datasets. Cls represents Classification. Seg represents Semantic Segmentation. Det represents Object Detection. Com represents Semantic Scene Completion. Rec represents Surface Reconstruction. CM represents Cross-Modal tasks. Pos means Pose estimation. Tra represents Object Tracking.

Year	Name	#Samples	#Categories	Types	Suitable tasks	Highlights
2012	KITTI [35]	Over 200K objects	8	RGB	Cls/Det/CM	Comprehensive outdoor driving dataset
2015	ModelNet [36]	12,311 models	40	CAD	Cls/Seg/Rec	Frequently used in classification and few-shot
2015	ShapeNet [37]	57,448 models	55	CAD	Cls/Seg	Commonly employed as the pre-training dataset
2015	SUN RGBD [38]	10,335 images	37	RGB-D	Seg/Det/Pos	A RGB-D scene understanding benchmark suite
2016	SceneNN [39]	100 scenes	-	RGB-D	Det/Rec/Pos	Using unique triangle meshes shape contour
2016	ObjectNet3D [40]	44,147 shapes	100	CAD	Det/CM/Pos	Well-aligned 2D-3D dataset
2016	S3DIS [41]	272 scans	13	Point	Cls/Seg/CM	Large-scale indoor space scanning dataset
2017	ScanNet [6]	1513 scenes	20	RGB-D	Cls/Seg/Com	Rich labels for scene understanding tasks
2017	Semantic3D.net [42]	Over 4B points	8	Point	Cls/Seg/Det	High quality resolution and scope outdoor dataset
2018	Pix3d [43]	10,069 3D-2D pairs	9	CAD	Rec/CM/Pos	Pixel-level image-shape pairs dataset
2019	ABC [44]	1M objects	-	CAD	Seg/Rec	Providing a benchmark for surface normal estimation
2019	ScanObjectNN [45]	2,902 objects	15	Point	Cls/Seg	Challenging real-world scenario with noise
2019	PartNet [46]	26,671 models	24	Points	Seg/Rec	Producing fine-grained multi-level 3D part objects
2020	RobustPointSet [47]	73,843	40	Mesh	Cls	Benchmark to evaluate the robustness of classifiers
2020	Waymo [48]	12M objects	-	Point	Det/CM/Tra	Suitable for cross-modal and transfer learning
2020	NuScenes [49]	1K scenes	23	Point	Det/CM/Tra	Containing additional annotations and scenes
2021	SensatUrban [50]	4B points	13	Point	Seg	Data collected by UAV over UK landscape
2022	STPLS3D [51]	62 scenes	18	Point	Seg/Det	Covering both real and synthetic aerial point clouds

- **Transformation immutability:** Point clouds remain immutable through rigid transformations such as rotation and translation.
- **Points interaction:** There are correlations, either strong or weak, between points in global and local regions.

2.3 Point Cloud Dataset

As deep learning continues to be explored in the 3D field, the need for 3D point cloud datasets is becoming increasingly stringent. It is no doubt that SSL is facilitated by the availability of complete, well-varied, and densely-labeled point cloud datasets. This section will list all commonly used point cloud datasets with brief descriptions and summarize them in Table 1 in terms of sample number, object categories, suitable tasks, and highlight contributions. It is worth mentioning that the point cloud data in this paper is in the broad sense that contains single frames and time series, individual objects and complex scenes, as well as synthetic and real scanned formats. Furthermore, there are a few automatic driving datasets containing extra modalities, like images or radar, forming complex traffic scenarios with point cloud data.

- **KITTI** [35] is a benchmark suite for autonomous driving vision tasks. The dataset was collected using several pieces of equipment, including four video cameras, a laser scanner, and a localization system. This comprehensive outdoor dataset includes not only point clouds but also stereo and optical flow data. For the 3D object aspect, there are more than 200 thousand annotated point cloud scenarios consisting of diverse cars and pedestrians, providing a novel challenging benchmark for 3D object detection and orientation estimation.
- **ModelNet** [36] is the most widely used 3D point cloud CAD dataset for object classification and few-shot learning. This dataset was aggregated and modified from previous smaller datasets by removing defective categories and unrealistic models. It contains a total of 12,311 single objects from 40 categories,

with each point composed of six dimensions of information, including XYZ spatial coordinates and RGB values.

- **ShapeNet** [37] is a relatively large-scale repository of 3D CAD objects frequently employed as a pre-training dataset. It contains more than 3 million samples categorized into 55 classes under the WordNet synsets [52] criteria. The annotations in the dataset are versatile, including rigid alignments, parts, physical sizes, and key points.
- **SUN RGBD** [38] is an RGB-D scene understanding benchmark suite containing 10,335 samples at a comparable scale to PASCAL VOC [53]. It has 146,617 2D polygons and 64,595 3D bounding boxes densely annotated to indicate object orientation, room layout, as well as scene category for overall scene awareness.
- **S3DIS** [41] is a 3D indoor venues dataset that scans 272 rooms in 6 areas overlaying a 6,000 m^2 area. It has 13 semantic categories labeled by fine-grained point-wise annotations carrying full 9D information, including XYZ, RGBs, and normalized location coordinates.
- **ScanNet** [6] is a 3D RGB-D dataset that comprises 2.5M views in 1,513 scenes acquired in 707 indoor environments. Various tests containing semantic voxel labeling and CAD model retrieval proved that ScanNet could provide quality data for 3D scene understanding.
- **ScanObjectNN** [45] was proposed as a collection of real-world indoor point cloud scenes to break the performance saturation of 3D object classification on synthetic data. This dataset introduces new challenges for 3D object classification due to the presence of background noise and occlusions that require networks' ability about context-based reconstructions and partial observations.
- **Waymo** [48] is a large autonomous driving dataset produced by Waymo in collaboration with Google Inc. The dataset consists of 1,150 urban and suburban geography scenes spanning 20 seconds, which

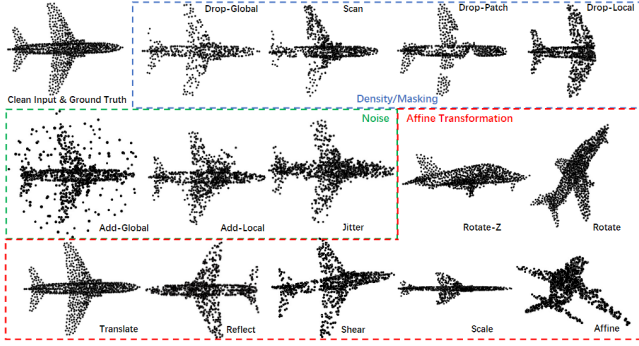


Fig. 3. Illustration of the commonly used data augmentation methods for point cloud data. There are a total of 14 sub-categories of data augmentation methods that could be classified as three general corruption families. The figure is adapted from [9].

are collected via well-synchronized and calibrated LiDAR and camera.

- **NuScenes** [49] is another remarkable multimodal dataset provided by the full sensor suite including cameras, radars, and LiDAR. Compared to other autonomous driving datasets, it contains additional annotations like pedestrian pose, vehicle state, and also scenes from nighttime and rainy weather.

2.4 Point cloud data augmentations

It is well known that data augmentation is a crucial technique for enhancing DNNs’ performance by increasing the amount and diversity of training samples. Especially for SSL tasks, it not only prevents the model from overfitting but also facilitates capturing robust and invariant representations of the point cloud under multiple transformations. In this section, we will introduce several commonly used data augmentation methods for point cloud data and compare the effectiveness of each approach via a specific metric.

Essentially, data augmentation is a process of generating new data by adding some interventions or corruptions based on not destroying the original semantic expression. In the point cloud field, data augmentation methods are applied based on the point cloud properties mentioned in Section 2.2 and can be classified into three general categories: density/masking, noise, and affine transformation [9]. These three corruption families could be further divided into 14 sub-categories displayed in Fig. 3.

Density/masking is the most frequent data augmentation method adopted in mask autoencoder (MAE) type SSL research [23], [54], [55]. Based on the principle that point cloud data is sparse with uneven density, randomly removing a certain percentage of points while preserving part of the semantic expression presents a challenging learning objective for such MAE-based tasks. On the contrary, the noise method is proposed to impose interventions on originally clean input so that it enhances the difficulty of feature extraction. While affine transformation, consisting of seven different approaches, leverages point cloud invariance characteristics to shift the spatial coordinates of each point, which causes the most significant impact on the input since basic position information varies completely.

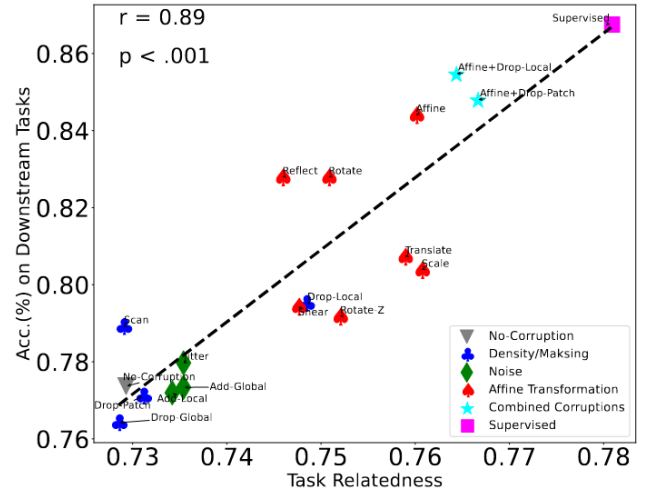


Fig. 4. Illustration of the relationship between task relatedness and classification accuracy on downstream tasks. r and p are the coefficients to measure the linear relationship and statistical significance for the Pearson correlation, respectively. The figure is adapted from [9].

Similar to SimCLR [24], Zhang *et al.* [9] investigated the effectiveness of the aforementioned data augmentation methods as pretext data preprocessing on downstream classification tasks. Task relatedness is employed as the evaluation metric to statistically measure the performance of SSL models on downstream tasks, which provides valuable advice for proxy data augmentation selection. Following [56], for each pretext task c , its task relatedness to downstream task t is defined as:

$$A_{c \rightarrow t} := \mathbb{E}_{x \in X} \mathcal{I}_t(R_c(E_c(x)), f_t(x)) \quad (1)$$

Where x is a sample in a point cloud dataset X . E_c is the model’s encoder pre-training on task c . R_c is a readout function, which indicates the classification head composed of several fully connected (FC) layers. f_t is the labeling function. \mathcal{I}_t is accuracy measurement estimating whether the downstream output $R_c(E_c(x))$ conform to the ground truth $f_t(x)$. Such accuracy-based task relatedness is the metric to measure the effectiveness of data augmentation methods.

To further explore the relationship between task relatedness and classification accuracy on downstream tasks, Pearson correlation coefficient r and p -value are utilized to estimate the linear relationship as well as statistical significance for Pearson correlation [57], respectively, where $|r| > 0.5$ refers to a strong relationship and $p < 0.05$ is considered statistically significant. Fig. 4 demonstrates the statistically significant linear relationship between task relatedness and classification accuracy on downstream tasks when $r = 0.89$ and $p < 0.001$. The results reveal a counter-intuitive fact that frequently used density/mask and noise-based data augmentation methods are ineffective for downstream tasks either in accuracy and task relatedness. Conversely, seemingly the most simple affine transformation enhances task relatedness to point cloud classification resulting in higher accuracy. Furthermore, the combined corruptions of affine transformation and mask can even approach the supervised

TABLE 2
Commonly used models to extract the point clouds feature.

Model	Year	Architecture	Contributions
PointNet [10]	2017	CNN	Pioneer in direct processing of raw point clouds with lightweight architecture
PointNet++ [11]	2017	CNN	Aggregating local neighborhood by multi-scale and multi-resolution sampling and grouping
VoxelNet [12]	2018	3D CNN	Partitioning disordered point clouds into regular voxels for local feature learning
DGCNN [13]	2019	Graph CNN	Constructing a dynamic local graph to capture edge features around a neighbor
PCT [58]	2021	Transformer	Successfully gaining the long-range dependencies between point patches
GANs [59]	2014	GAN	Generating synthetic data through adversarial training

benchmark. Hence, using affine transformation-based methods for data augmentation is preferable for point cloud data preprocessing in SSL pre-train.

2.5 Commonly used models for point cloud learning

Although the SSL idea can be extended from language and images to point clouds, different data peculiarities lead to distinct network structures for corresponding preprocessing. For instance, traditional CNN networks cannot handle irregular and discrete point cloud data well since there is no guarantee that a corresponding point exists at the same relative position of the convolution. In this section, we introduce five point cloud networks that are frequently used as feature extraction encoders in the self-supervised paradigm and summarize their respective characteristics in Table 2 for intuitive presentation.

2.5.1 PointNet

To reduce data size and complexity, Qi *et al.* proposed PointNet [10], which is the pioneering work to extract features directly on the raw, unprocessed point cloud. It is widely deployed as the feature extractor [60]–[62] in the SSL framework due to its simple and lightweight network structure. Taking advantage of the point permutation invariance, PointNet aligns the input points to a canonical space and aggregates global features by a symmetric function such as max pooling.

However, it fails to capture local structures induced by the metric space in which the points reside, thereby limiting its ability to recognize fine-grained patterns and generalize to complex scenes. The updated version PointNet++ [11] was then put forward several months later. It adopts multi-scale, multi-resolution sampling, and grouping strategies to propagate features from one level to another, which improves the feature learning ability further. Furthermore, the point patch generation strategy combining Farthest Point Sampling (FPS) and K-Nearest Neighbor (KNN) provides a template for point cloud cropping preprocessing for subsequent studies [54], [55], [63].

2.5.2 VoxelNet

VoxelNet [12] is a generic point-specific network that uses voxels, a kind of finite unit cube, to divide and access a local representation of the point cloud for 3D detection tasks [64]–[66]. This network partitions disordered point clouds and performs feature learning in quantified and fixed-size 3D structures. One innovation is the stacking Voxel Feature Encoding (VFE) layers which encode interaction between points within a voxel and grasp descriptive appearance information. The output of each VFE layer is the concatenation

of point-wise features and locally aggregated features so that local features are better captured. However, the expensive computation of voxel construction and quantization artifacts constrain the model capturing high-resolution or fine-grained representation.

2.5.3 DGCNN

A point with its neighbors can reflect the geometry property of a local point cloud. Such a local community relationship could be expressed easily by a graph network. Therefore, Wang *et al.* proposed a dynamical graph-based CNN network (DGCNN) [13] that encodes the edges feature between vertices. Instead of learning point representations directly, DGCNN depicts the interactions between points and their connection edges in both Euclidean and semantic space and alters the graph structure dynamically if the learnable parameters are updated. This graph network-based architecture has served as a backbone in many subsequent point cloud SSL models with good results [61], [62], [67].

2.5.4 GANs

Generative Adversarial Networks (GANs) [59] are a widely used framework in reconstruction-based pretext tasks for point cloud knowledge mining. GANs consist of two sub-modules: the generator, which generates point clouds similar to the training data, and the discriminator, which distinguishes between generated and real point clouds. These two modules are trained under an adversarial paradigm without any supervision. The framework can be formulated as a two-player minimax game:

$$\min_G \max_D E_{x \in X} [\log(D(x))] + E_{z \in Z} [\log(1 - D(G(z)))] \quad (2)$$

where D and G denotes the discriminator and the generator in GAN. X and Z represent the data and noise distribution, respectively.

2.5.5 Transformers

Transformers are currently the most prevalent architectures in all fields. They benefit from the multi-head self-attention mechanism, which allows them to easily capture long-range dependencies between point patches and discover implicit regional correlations. The state-of-the-art performance of SSL point cloud classification and part segmentation is achieved by transformer-based models such as the one proposed by Zhang *et al.* [63]. Furthermore, point cloud transformer (PCT) [58], a variant adapted specifically for point clouds, enhances local feature extraction with the support of farther point sampling and nearest neighbor search. Such a design further improves performance on various downstream tasks.

2.6 Pseudo labels

To address the absence of ground truth labels, it is imperative to generate a pseudo label from the raw point cloud input. This enables calculation of loss via comparison between output of the pretext task and pseudo labels, which is then used for encoder updating via backpropagation. Normally, information contained in pseudo label is more considerable than human tags. For instance, label ‘airplane’ could only indicate shape of object without other descriptions like color, pose, and differences from other samples in same category. Instead, aforementioned attributes are implicitly involved in point cloud itself and could be captured as pseudo label in SSL tasks. Therefore, pseudo label is more reliable and informative source for pretext task to learn point cloud representation.

In most reconstruction-based pretext tasks, pseudo label is point cloud itself which provides rebuild objective for pretext task. In contrast-based methods, pseudo label is multidimensional matrix typically generated using clustering methods such as memory bank [68], online dictionary [25], and prototype approaches [26], representing mean and variance of all or part of features of point cloud dataset. For some alignment-based prediction or motion-based tasks pre-trained on temporal point cloud datasets, pseudo label is geometric information like position, pose, and orientation in several frames before and after.

2.7 Loss functions

Moreover, selecting an appropriate and easily-differentiable loss function is critical to facilitate backpropagation and encoder optimization. In the case of reconstruction-based pretext tasks, Chamfer distance (CD), which is a symmetric function used to measure the similarity between two point sets, is commonly employed to assess the distances between each point in one set and its corresponding nearest point in the other set. More formally, for two non-empty subsets X and Y , Chamfer distance $d_{CD}(X, Y)$ is defined as:

$$d_{CD}(X, Y) = \frac{1}{|X|} \sum_{x \in X} \min_{y \in Y} \|x - y\|^2 + \frac{1}{|Y|} \sum_{y \in Y} \min_{x \in X} \|x - y\|^2 \quad (3)$$

Here, x and y represent the points in the reconstruction point set X and the original input point set Y , respectively. $\|\cdot\|$ denotes the L2 distance between two points and $|\cdot|$ refers to the number of points. The smaller the CD value, the more similar the two point sets are, and the better the SSL algorithm performs.

For contrast-based pretext tasks, the objective is to discriminate the similarities and differences between each point cloud sample on the overall semantic understanding level. Diversity data augmentation is applied to generate positive samples that are similar to the input point cloud and negative samples that are transformed from other point clouds. Therefore, it requires a cross-entropy variant loss function to encourage the positive samples to be close to each other and vice versa. InfoNCE, where NCE stands for Noise-Contrastive Estimation, is a contrastive loss function that estimates the mutual information between a pair of samples. It can be formulated as:

$$L_q = -\log \frac{\exp(q \cdot k_+ / \tau)}{\sum_{i=0}^K \exp(q \cdot k_i / \tau)} \quad (4)$$

where q indicates the encoded query (feature). k indicates a set of $K + 1$ encoded samples $\{k_0, k_1, k_2, \dots, k_K\}$, which could be regarded as the historical samples prototype. And τ is the temperature parameter controlling the sharpness of the distribution. Assuming there is only one positive sample k_+ in the set k matching the query q , the others K samples are all negative. InfoNCE aims to assign the query q into the positive class k_+ in the $K + 1$ classification problem [25]. In other words, the loss function tries to maximize the logits of $q \cdot k_+$ and minimize the value of the denominator. The only difference between InfoNCE and cross-entropy is that the value of K means the number of negative samples for InfoNCE, while it represents the number of dataset categories in cross-entropy.

3 SELF-SUPERVISED LEARNING PRETEXT TASKS FOR POINT CLOUD

As shown in Fig. 2, we classify the current point cloud SSL pretext tasks into four general categories based on the nature of the point cloud that each method exploits: reconstruction-based, contrast-based, alignment-based, and motion-based methods. These categories can be further subdivided into fine-grained specific tasks according to the varying feature-utilizing aspects. The following sections will elucidate the principles and peculiarities of various proxy tasks by presenting representative examples with illustrative formulas or figures. Notably, some pretext tasks may comprise multiple sub-categories, so such works will be raised in various sections.

3.1 Reconstruction-based methods

Reconstruction-based methods are the most prevalent SSL proxy tasks for point clouds. Such methods learn the point cloud representation by reconstructing the corrupted point cloud as close as possible to the original entire input. Not only global features but also the mapping between local and global is learned during the reconstruction process. According to the different types of corruption and reconstruction objects, the reconstruction-based methods can be divided into six sub-categories: mask recovery, spatial restoration, point sampling, disentanglement, deformation reconstruction, and generation and discrimination. In the following subsections, we will introduce the details of each sub-category with representative examples and summarize the contribution of each method in Table 3.

3.1.1 Mask recovery

The primary concept of reconstruction is to mask a portion of the point cloud and recover such missing components via the encoder-decoder architecture. Similar to the image inpainting task [83] and Mask AutoEncoder (MAE) [66], the encoder is required to capture the local geometric structure representation and the regional relations during the restoration process. Generally speaking, the better the reconstruction, the more effective the learned features.

TABLE 3
Summary of reconstruction-based point cloud SSL pretext tasks. D & G is an abbreviation for Generation and Discrimination.

Year	Method	Sub-categories	Contributions
2021	Point-BERT [55]	Mask recovery	Reconstructing the missing point token upon the BERT-style transformer
2022	Point-MAE [54]	Mask recovery	Shifting the masked tokens to the decoder to avoid early leakage
2022	MaskSurf [63]	Mask recovery	Estimating the surfel position and per-surfel orientation simultaneously
2022	Voxel-MAE [65]	Mask recovery	Performing additional binary voxel classification for complicated semantics awareness
2019	3D jigsaw [62]	Spatial restoration	Rearranging randomly disorganized point clouds
2019	CloudContext [69]	Spatial restoration	Predicting the relative structural position between two given patches
2020	Orientation estimation [61]	Spatial restoration	Predicting and recovering the rotation angle around an axis
2019	PU-GAN [70]	Point sampling / D & G	Utilizing a self-attention unit for feature aggregation quality enhancement
2021	SSPU-Net [71]	Point sampling	Leveraging the shape coherence between input sparse and generated dense point cloud
2022	UAE [72]	Point sampling	Gaining both advanced semantic information and basic geometric structure
2022	SPU-Net [73]	Point sampling	Integrating self-attention with graph convolution network for context feature extraction
2022	PUFA-GAN [74]	Point sampling / D & G	Employing a graph filter to extract the high frequency points of sharp edges and corners
2022	SSAS [75]	Point sampling	Achieving magnification-flexible point clouds upsampling
2022	Pose Disentanglement [76]	Disentanglement	Uncoupling content and pose attributes in partial point clouds
2022	CP-Net [77]	Disentanglement	Disentangling the point cloud into contour and content ingredients
2022	MD [78]	Disentanglement	Separating the mixing point cloud into two independent objects
2018	FoldingNet [79]	Deformation reconstruction	Stretching a 2D grid lattice to reproduce the 3D surface structure
2021	Self-correction [80]	Deformation reconstruction	Recovering the shape-disorganized point regions
2021	DefRec [81]	Deformation reconstruction	Performing deformation on 2D grids to fit an arbitrary 3D object surface
2018	PC-GAN [82]	D & G	Employing a hierarchical and interpretable sampling strategy
2019	RL-GAN [83]	D & G	Introducing a reinforcement learning agent to control the GAN
2019	TreeGCN [84]	D & G	Leveraging the ancestor information to boost the representation of the point
2022	MaskPoint [85]	D & G	Performing simple binary classification as the proxy task

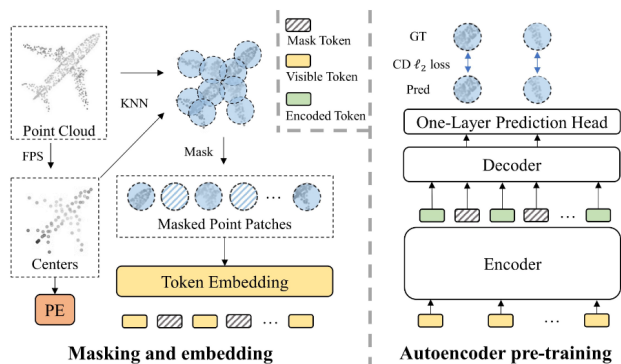


Fig. 5. The general pipeline of Point-MAE. (1) The process of masking and embedding is demonstrated on the left. The point cloud patches are generated by the FPS-KNN technique and masked randomly. Both visible and mask patches are mapped to the corresponding token through PointNet-based embedding layers. Also, the Position Embedding (PE) is obtained by mapping the center coordinates to the embedding dimension. (2) The autoencoder pre-training is shown on the right. The encoder only processes the visible tokens while the mask tokens are shifted and added as the input sequence of the encoder to reconstruct the masked point patches. This figure is adapted from [54].

Point-BERT [55], inspired by BERT [16], designed a point-specific tokenizer built upon discrete Variational AutoEncoder (dVAE) to map point patches into discrete point tokens that imply meaningful local geometric patterns. A portion of the input is then randomly masked out, and a BERT-style transformer is trained to reconstruct the missing point token under the supervision of point tokens obtained by the tokenizer. However, the tokenizer should be pre-trained advanced, and Point-BERT over-relies on the auxiliary contrastive learning as well as data augmentation. To address aforementioned issues, Pang *et al.* proposed Point-MAE [54] as a neat and efficient scheme of mask autoencoder shown in Fig. 5. Concretely, Point-MAE employs the standard transformer as its backbone with asymmetric encoder-decoder architecture to process random masking points with a high ratio (60%-80%). The mask tokens are

shifted from the input of the encoder to the lightweight decoder, which saves considerable computation, and more significantly, avoids early leakage of location information. To further capture local geometric information, Zhang *et al.* introduced Mask Surfel Prediction (MaskSurf) [63], which estimates the surfel position (i.e., points) and per-surfel orientation (i.e., normals) simultaneously. Such a two-head pre-training paradigm was justified to capture more effective representations than a reconstruction-only pretext. Likewise, Voxel-MAE [65] transforms point clouds into volumetric representations and applies the range-aware random masking strategy on the voxel grid. Except for reconstructing the occupancy value of masked voxels, a supplementary binary voxel classification task distinguishing whether the voxel contains point clouds boost the model to figure out complicated semantics.

3.1.2 Spatial restoration

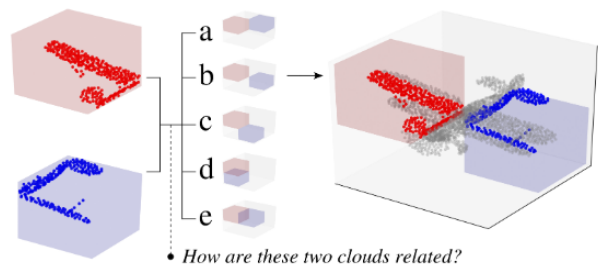


Fig. 6. The illustration of the CloudContext pretext task. The pre-training model is enforced to estimate the spatial relevance between two given point cloud segments from six provided categories. In this case, the exact relation of these two components is "the reading part is diagonally above the blue part". This figure is adapted from [69].

The point cloud is the coordinate set containing abundant spatial information that describes the structural distribution of objects and the environment in Euclidean space. It is natural to exploit such rich spatial knowledge as the

supervision signal in the pretext tasks to learn favorable representations.

Sauder *et al.* [62] proposed a 3D version of the jigsaw pretext to rearrange point clouds whose parts have been randomly disrupted and displayed by voxels along the axes. The goal of this pretext is to restore the original position of each patch labeled by voxel ID from the state of chaotic and disorderly distribution. Likewise, they further produced CloudContext [69] to forecast the spatial relevance between two point cloud segments. As shown in Fig. 6, the pre-training model is trained to predict the relative structural position between two given patches from the same object, which utilizes the innate flexible attribute of point clouds as they are not restrained by a discrete grid. By doing so, powerful per-point features could be accessed in an easy-to-implement unsupervised manner without expansive computation. Orientation estimation [61] was another simple but effective proxy task to capture the spatial information of point clouds. Thanks to the convenience of canonical orientation provided in most datasets, the orientation estimation pretext task aims to predict and recover the rotation angle around an axis via matrix multiplication. Such a pretext requires a high-level holistic understanding of shapes and obviates the need for manual annotations cleverly.

3.1.3 Point upsampling

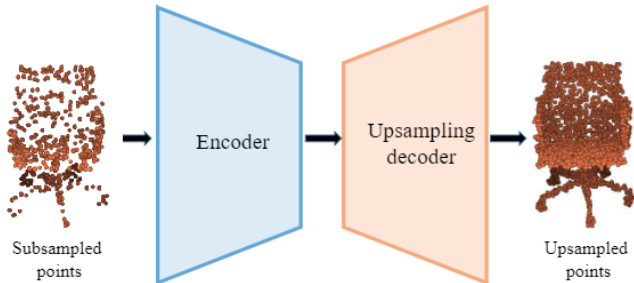


Fig. 7. Overview of Upsampling AutoEncoder. The input point cloud is subsampled by a random sampling strategy and then fed into the encoder to extract point-wise features. The decoder is adopted to reconstruct the original point cloud with offset attention based on the learned representation. This figure is adapted from [72].

Point upsampling is the operation to upsample sparse, noisy, and non-uniform point clouds to generate a dense, complete, and high-resolution point cloud, which is challenging but also beneficial for the model to capture implicit geometric representations of the underlying surface.

PU-GAN [70] was a pioneer SSL upsampling paradigm formulated based on a generative adversarial network (GAN) [59] to grasp a diverse range of point distribution from the latent space and upsample points over patches. An up-down-up unit is embedded in the generator to expand point features as well as a self-attention unit for feature aggregation quality enhancement. The discriminator is inspired to gain inherent patterns and improve the uniformity of output generation according to a compound loss including adversarial, uniform, and reconstruction terms. Motivated by PU-GAN, Zhang *et al.* proposed the Upsampling AutoEncoder (UAE) [72] to gain both advanced semantic information and basic geometric structure from the subsampled point cloud. As shown in Fig. 7, the encoder is devised

to perform point-wise feature extraction on the subsampled point cloud, and the upsampling decoder is designed to reconstruct the original dense point cloud with offset attention [58] to refine global shape structure. Liu *et al.* [73] proposed a coarse-to-fine reconstruction framework, dubbed SPU-Net, integrating self-attention with graph convolution network (GCN) for context feature extraction and generating fine point sets with hierarchically learnable 2D grids. Zhao *et al.* [71] introduced SSPU-Net leveraging the shape coherence between input sparse and generated dense point cloud as well as image-consistent loss among multi-view rendered images to capture the latent pattern of underlying point structure. PUFA-GAN [74], a frequency-aware framework, utilized a graph filter to extract the high frequency (HF) points of sharp edges and corners so that the discriminator could focus on the HF geometric properties and enforce the generator producing more uniform and neat upsampled point cloud. To get rid of fixed upsampling factor restriction, Zhao *et al.* [75] presented a self-supervised arbitrary-scale (SSAS) framework with a magnification-flexible upsampling strategy. Instead of direct mapping from sparse to dense point clouds, the proposed scheme seeks the nearest projection points on the implicit surface for seed points via two functions, which are exploited to estimate the projection direction and distance respectively.

3.1.4 Disentanglement

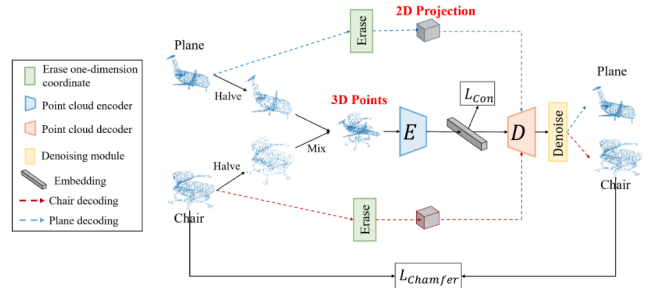


Fig. 8. The schematic of Mixing and Disentangling (MD) pretext. The two input point clouds are separately halved and mixed into a hybrid object feeding to the encoder E to mine the geometry-aware embedding. The *Erase* operation is applied to obtain the 2D projection from both original input point clouds simultaneously. The instance-adaptive decoder D receives the embedding with two partial projections as input to disentangle the blended shape into the original two point clouds. The chamfer distance is used to measure the reconstruction error between generated point clouds and the original ones. This figure is adapted from [78].

The model pre-trained under the SSL paradigm usually prefers to grasp the low-level geometric features of point clouds, such as pose, contour, and shape information but neglects the high-level semantic content understanding, which leads to unsatisfactory performance in downstream tasks like object classification that require global discriminative capability. To tackle this issue, disentanglement-based SSL pretexts were proposed to separate the low-level geometric features from the high-level semantic embedding and feature extraction is performed on various content via distinct modules to obtain hierarchical representations.

Tsai *et al.* [76] proposed a self-supervised disentanglement framework that uncouples content and pose attributes

in partial point clouds to enhance both geometric and semantic feature abstraction. Two encoders are employed to learn the content and multi-view poses individually, where the gained pose representation should predict the viewing angle and navigate the partial point cloud reconstruction cooperated with the content from another specific view. Likewise, Xu *et al.* [77] presented a universal Contour-Perturbed Reconstruction Network (CP-Net) that disentangles the point cloud into contour and content ingredients, where a concise contour-perturbed augmentation unit is exploited on the contour component while retaining the content part of the point cloud. Therefore, the self-supervisor is able to concatenate the content component for advanced semantic comprehension.

Different from the above two pretexts, Mixing and Disentangling (MD) [78] blends two disparate point shapes into a hybrid object and attains geometry-aware embedding from the encoder. An instance-adaptive decoder is then leveraged to restore the original geometries based on the obtained embedding by disentangling the mixed shape. As shown in Fig. 8, except for the main encoder-decoder structure, the proposed scheme also encompasses a coordinate extracting operation “Erase,” which randomly drops one-dimension coordinate of each point to provide an extra 2D partial projection for the encoder to better reconstruct the original two-point cloud shapes.

3.1.5 Deformation reconstruction

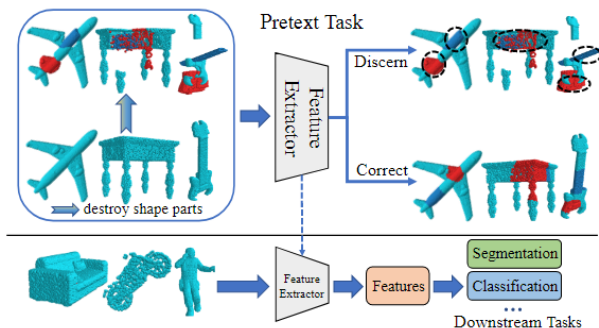


Fig. 9. The demonstration of shape self-correction pretext. The input point cloud is firstly preprocessed by a shape-disorganizing module to generate a deformed point cloud and then fed to the encoder to grasp the geometry-aware representation. Two separate task heads are constructed to distinguish and segment points belonging to distorted parts and subsequently reconstruct partial-deformed objects to their initial status. The well-trained feature extractor is transferred to downstream tasks to estimate the feature capturing ability. This figure is adapted from [80].

Point cloud deformation is a common phenomenon in real-world data scanning, which is usually caused by object distortion, sensor noise, or external occlusion. It has been discovered that reconstructing the original point cloud from the artificially deformed one, implemented by adding Gaussian noise or local translation, supports the model in grasping geometric perception as well as context awareness of the point cloud.

Chen *et al.* [80] proposed a shape self-correction pretext to mine the implicit geometric embedding of point clouds. The pretext assumes that a robust shape representation

could identify and correct distorted regions of a shape. As shown in Fig. 9, the proposed scheme imposes destruction over certain shape regions by a shape-disorganizing module and sends the deformed point cloud to the feature extractor for embedding learning. Two task heads are built separately to discern the distorted components and further restore them to their original normal shapes for fine-grained geometric and contextual feature explorations.

Achituve *et al.* [81] proposed the first study of SSL for domain adaptation (DA) on point cloud field via Deformation Reconstruction (DefRec). By mapping the dislocating points to their original location, the model is capable of obtaining the latent statistical structure of input point cloud objects. Moreover, the distribution gap between source and target domains is bridged by the learned underlying representation since they are invariant to distribution shift.

FoldingNet [79] presented a novel folding-based decoder to perform deformation on the canonical 2D grid to fit an arbitrary 3D object surface. Instead of deforming the point cloud, the folding operation exerts a “virtual force” induced by the embedding captured from input to stretch a 2D grid lattice to reproduce the 3D surface structure and tackle issues caused by point cloud’s irregular attributes by applying implicit 2D grid constraint.

3.1.6 Generation and discrimination

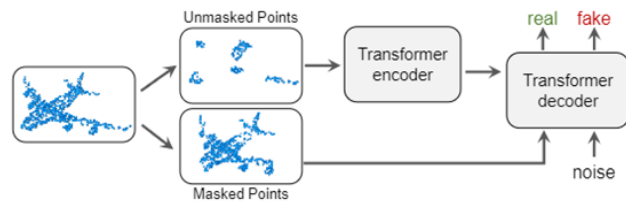


Fig. 10. The general pipeline of the Mask-Point model. The reconstruction challenge is reformulated as a discriminative pretext to determine whether the source of the extracted sample is a masked point cloud or a random noise. The figure is adapted from [85].

The generation and discrimination pretext was a unique paradigm that replaced the comparison between the generated and input point clouds with a discriminator module that distinguishes whether the fed point cloud is reconstructed from noise distribution or truly sampled. During the adversarial training process, the generator (encoder) and discriminator (decoder) compete with each other and are updated alternatively so that both components can be transferred as initial networks for downstream tasks.

The point cloud GANs variation models are representative of generation and discrimination approaches. PC-GAN [82] is a modified framework specifically for point clouds that employs a hierarchical and interpretable sampling strategy inspired by Bayesian and implicit generative models to tackle the issue of missing constraints on the discriminator. Sarmad *et al.* [83] introduced a reinforcement learning (RL) agent to control the GAN to grasp the implicit representation from noisy and partial input to generate high-fidelity and entire point clouds. Meanwhile, applying an RL agent to seek the best-fit input of GAN to produce low-dimension latent embedding relieves the challenge of unstable GAN training. Shu *et al.* [84] introduced a tree-structured graph

TABLE 4
Summary of contrast-based point cloud self-supervised learning pretext tasks.

Year	Method	Sub-categories	Contributions
2020	Info3D [86]	Object contrast	Maximizing the mutual information between objects and their transformations
2022	AFSRL [87]	Object contrast	Imposing data-level augmentation and feature enhancement simultaneously
2019	Contrasting and clustering [88]	Object contrast	Solving the part contrast and object cluster tasks consecutively
2021	Hard negatives [89]	Object contrast	Leveraging self-similar point cloud patches facilitating hierarchical context primitives capturing
2020	PointContrast [90]	Scene contrast	Obtaining dense features at the point-level on complex scenes by point contrast
2021	Contrastive Scene Contexts [91]	Scene contrast	Introducing ShapeContext local descriptor and achieving data-efficient
2021	CoCoNets [92]	Scene contrast	Mapping RGB-D images to 3D point scenarios by optimizing view-contrastive prediction
2020	P4Contrast [93]	Scene contrast	Utilizing the synergies between two modalities for better feature extraction
2021	DepthContrast [94]	Scene contrast	Applying the Instance Discrimination method on depth maps

convolution network (TreeGCN) as the generator leveraging ancestor information to boost the representation of the point which is more efficient in computation than neighborhood features adopted in regular GCNs. PU-GAN [70] and PUFA-GAN [74], both employed GANs-based models to generate dense and uniform point clouds with disparate innovative modules for feature aggregation element enhancement and high-frequency point filtering, respectively.

Liu *et al.* [85] proposed a discriminative mask pretraining transformer framework, MaskPoint, which combines mask and discrimination techniques to perform simple binary classification between masked object points and sampled noise points as the proxy task. As shown in Fig. 10, the original complete point cloud is divided into 90% masking portions and a 10% visible set. Two kinds of query, where the real is sampled from masked point clouds while the fake is derived from random noise, are fed to the decoder to distinguish the query source. During the discrimination process, the model is required to deduce the full geometry from small visible portions.

3.2 Contrast-based methods

Contrastive learning is a popular mode of SSL that encourages augmentations of the same input to have more comparable representations than the views of different inputs. The general approach is to expand the views of input point clouds (anchors) by various data augmentation techniques to make the positive samples augmented from the same anchor more similar to the negative samples from different anchors in the feature space. In this section, we will introduce SSL contrast-based methods for point clouds with representative examples and summarize each method’s contribution in Table 4.

3.2.1 Object contrast

Traditional contrastive learning research focuses on instance-wise objects, where the priority is on overall semantic learning through discriminative pretext tasks that capture context similarity and difference of point clouds. Therefore, such an object-contrast paradigm performs data augmentation on relatively large patches or whole single point objects to capture global geometric awareness.

Sanghi [86] proposed Info3D, which takes inspiration from Contrastive Predictive Coding [95] and Deep InfoMax [96], to obtain rotation-insensitive representation by maximizing mutual information between 3D objects and their local chunks as well as geometrically transformed versions. Lu *et al.* [87] proposed the Augmentation Fusion Self-Supervised Representation Learning (AFSRL) framework,

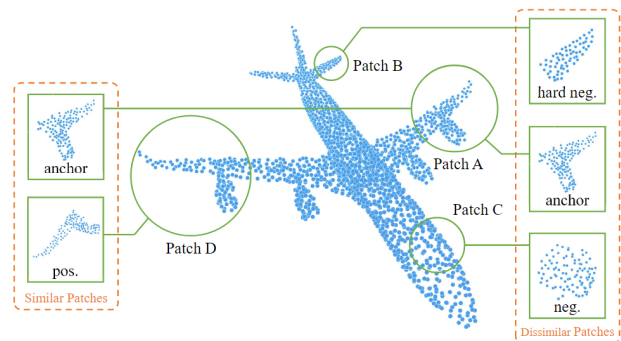


Fig. 11. The illustration of a self-contrastive paradigm. Patch D is selected as the anchor and the symmetrical part Patch B is the positive sample. Patch B and C are the negative samples, where Patch C is hard to distinguish due to its comparative similarity to the anchor. The figure is adapted from [89].

which imposes data-level augmentation and feature enhancement simultaneously to construct a stable and invariant point cloud embedding. The correspondence between augmented pairs is acquired, and the invariant semantic is maintained under perturbations during two aspects augmentations. Zhang *et al.* [88] introduced a simple two-phase unsupervised GCN framework, named contrasting and clustering, to capture superior point embedding by solving part contrast and object cluster tasks consecutively. Du [89] presented a self-contrastive paradigm leveraging self-similar point cloud patches within a single point cloud to facilitate local shape and global context primitives capturing. As shown in Fig. 11, according to the nonlocal self-similar property of the point cloud, where regional geometric keeps invariant after affine transformation, the self-similar point cloud patches are treated as positive samples otherwise negative based on the inferred similarity score. Moreover, hard negative samples, close to positive samples in the representation space, are sampled for more discriminative and expressive representation learning.

3.2.2 Scene contrast

Different from the object-contrast, the scene-contrast paradigm concentrates on scene-level contrastive learning to grasp broader environmental context and neighborhood perception, which is more challenging but also more relevant to real-world complex scenarios.

To address the domain gap concern that it is insufficient to capture a global representation from object instances, Xie *et al.* [90] proposed PointContrast, a sparse residual U-Net

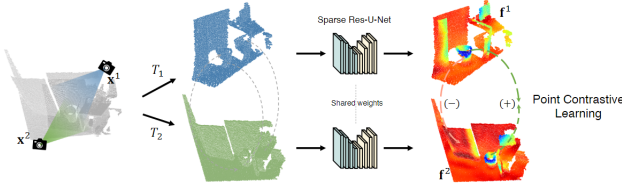


Fig. 12. The illustration of PointContrast. Contrast is performed at the point-level between two transformed point clouds, where the positive samples are the matched points while the negative samples are the unmatched points across two views. The figure is adapted from [90].

based framework aiming to obtain dense features at the point-level on complex scenes. As shown in Fig. 12, two views x^1 and x^2 are produced from a complicated point cloud scene input, where pairs of the point-level corresponding match are computed between these two views as the positive samples. Two rigid transformations T^1 and T^2 are utilized to increase the pretext’s difficulty which demands the network to learn the invariant embedding under random geometric shift. The contrastive loss is defined to shorten the distance between the matched points and enlarge the distance of mismatched points of two overlapping partial scans so that the pre-training model can capture local description and be universally pertinent to various advanced 3D understanding downstream tasks. However, PointContrast only considered point correspondence matching but ignored the spatial configurations and contexts in a scene, e.g., relative pose and distance, therefore confining scalability and transferability. To remedy this shortcoming, Hou *et al.* [91] presented Contrastive Scene Contexts to fuse spatial information into pre-training objects by introducing ShapeContext local descriptor [97] partitioning and performing contrastive learning in each region. Such simple improvement modifies downstream performance and achieves data-efficient that only employs 0.1% of point labels to reach the same effect as full supervision.

Continuous Contrastive 3D Networks (CoCoNets) [92] aimed to infer latent scene representation by mapping RGB-D images to 3D point scenarios by optimizing view-contrastive prediction. P4Contrast [93], another RGB-D bimodal SSL framework, proposed contrasting “pairs of point-pixel pairs” providing additional flexibility for hard negatives creation to utilize the synergies between two modalities for better feature extraction. DepthContrast [94] circumvents the need for point correspondences and instead applies the Instance Discrimination [68] method on depth maps combined with a momentum encoder to grasp the geometric perception for point cloud scenes.

3.3 Alignment-based methods

Point cloud representation is generally invariant to transformations in terms of time flow, spatial motion, multi-view photography, etc. Based on this imperative property, alignment-based methods have been proposed to learn the implicit embedding of point clouds by preserving the coherence of point features in spatiotemporal consistency, multi-view alignment, and multimodal fusion. In the following content, we will demonstrate the details of these sub-

categories with representative examples and summarize the contribution of each method in Table 5.

3.3.1 Multi-view alignment

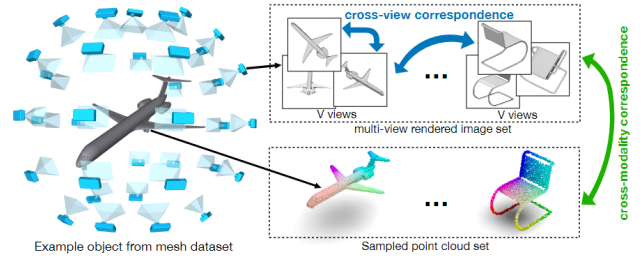


Fig. 13. The schematic of cross-modality and cross-view correspondences. The 3D point cloud objects and corresponding pairs of multi-view rendered images are sampled from the same mesh input, respectively. The relation of diverse views is captured as the supervision signal by sustaining the alignment among multi-view and cross-domain representations. The figure is adapted from [99].

Compared to direct processing and feature extraction on 3D point clouds, projecting point clouds into 2D images for dimension reduction and utilizing mature image networks as well as 2D SSL technologies is relatively more accessible. To ensure that the learned embedding sufficiently represents the entire 3D point cloud object or scene, multi-view alignment pretexts are necessary to preserve the integrity and uniformity of obtained point cloud features.

Info3D [86] was a pioneer in research aimed at obtaining rotation-insensitive representation by maximizing mutual information between 3D objects and their local chunks for patch-level consistency. Occlusion Completion (OcCo) [60] combined the idea of mask recovery shielding and restoring occluded points in a camera view for better spatial and semantic properties comprehension. Similarly, Yang *et al.* [98] introduced an SSL multi-view stereo structure generating prime depth map as pseudo-labels and refined such self-supervision from neighboring views as well as high-resolution images by multi-view depth fusion iteratively. Furthermore, the correspondence of pixel/point of the point clouds and its corresponding multi-view images should be aligned for cross-modality consistency. Jing *et al.* [99] proposed a novel SSL framework leveraging cross-modality and cross-view correspondences to jointly grasp both 3D point cloud and 2D image embedding concurrently. As shown in Fig. 13, point cloud objects and comparable pairs of multi-view rendered images are sampled from the same mesh input, respectively. In addition to 2D-3D consistency, the contrastive notion is adopted into cross-view alignment that shortens intra-object distance while maximizing inter-object discrepancy of distinct rendered images. Similarly, Tran *et al.* [100] presented a dual-branch schematic not only agreeing upon fine-grained pixel-point local representation but also encouraging 2D-3D global feature distribution as approaching as possible by exploiting knowledge distillation.

3.3.2 Spatiotemporal consistency

Unlike previous methods, the spatiotemporal approach is more concerned with long-range spatial and temporal invariance before and after point cloud frames, which are 4D

TABLE 5
Summary of alignment-based point cloud self-supervised learning pretext tasks.

Year	Method	Sub-categories	Contributions
2020	Info3D [86]	Multi-view alignment	Maximizing the mutual information between objects and their transformations
2021	OcCo [60]	Multi-view alignment	Shielding and restoring occluded points in a camera view
2021	Multi-view stereo [98]	Multi-view alignment	Generating prime depth map as the self-supervision signal
2021	Cross-view [99]	Multi-view alignment	Jointly grasping both 3D point cloud and 2D image embedding concurrently
2022	Multi-view rendering [100]	Multi-view alignment	Encouraging the 2D-3D global feature distribution similar
2021	Order prediction [101]	Spatiotemporal consistency	Sorting the temporal order of sampled and disorganized point cloud clips
2021	STRL [102]	Spatiotemporal consistency	Dual-branch network to predict the representation of another temporally correlated input
2022	Futruue prediction [103]	Spatiotemporal consistency	Forecasting future point cloud scenes with lightweight model
2020	PointPainting [104]	Multimodal fusion	Projecting LiDAR points into the semantic segmentation diagram for traffic scenes
2021	PointAugmenting [105]	Multimodal fusion	Replacing sub-optimal segmentation scores with high-dimension CNN features
2022	DeepFusion [64]	Multimodal fusion	Exploiting cross-attention to dynamic capture long-range correlations of image-LiDAR pairs

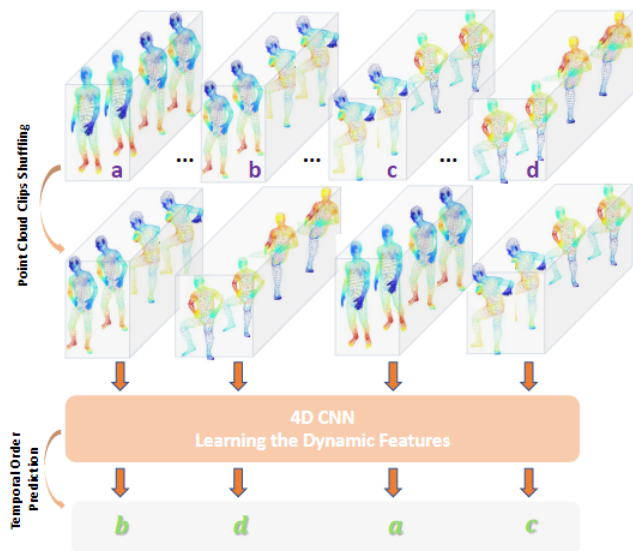


Fig. 14. The demonstration of point cloud sequence order prediction. The first row is the uniformly sampled point cloud clips from the continuous point cloud sequence. Then randomly disrupt the order of these segments and enter them into 4DCNN in the second row to master the dynamic features of human action, which are leveraged to forecast the original permutations in a self-supervised manner. The figure is adapted from [101].

data (XYZ coordinate + temporal dimension), to capture the intrinsic characteristics of dynamic sequences that are absent in static 3D point data.

Motivated by the success of Xu *et al.*'s work [106] in video SSL, Wang *et al.* proposed the first SSL scheme to gain effective temporal embedding on dynamic point cloud data by sorting the temporal order of sampled and disorganized point cloud clips. As shown in Fig. 14, a few static point cloud frames are uniformly sampled and disordered as the input of a 4D CNN to capture significant campaign information by restoring the disrupted time fragments to correct order on an unannotated large-scale sequential point cloud action recognition dataset. Another spatiotemporal representation learning (STRL) [102] framework, inspired by BYOL [107], designed a dual-branch pipeline referred to as online and target networks to collaborate and promote each other. Specifically, the online network is enforced to predict the target network representation of another temporally correlated input, which is augmented by random spatial transformation, for spatiotemporal invariant contextual cues extraction. Taking training and inference time into account,

Mersch *et al.* [103] presented an innovative 3D spatiotemporal convolutions encoder-decoder neural network consisting of fewer parameters to predict future point cloud scenes. Such a lightweight model concatenates range images as input to estimate forthcoming range images and per-point scores in multiple future steps so that aggregate spatial and temporal scene information can be captured simultaneously.

3.3.3 Multimodal fusion

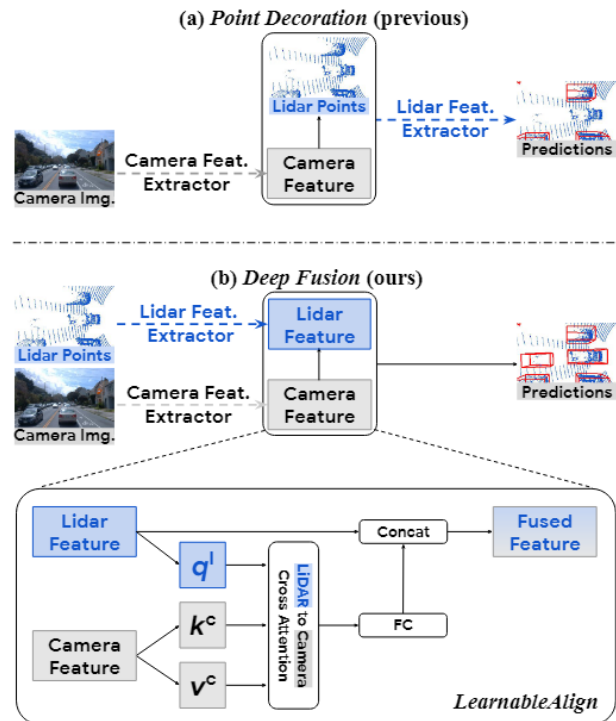


Fig. 15. The demonstration of point decoration and deep fusion. (a) Previous cross-modal paradigms [92], [99] decorated LiDAR points with camera feature on input-level for 3D detection. (b) DeepFusion [64] fused the camera and LiDAR features extracted by respective encoders on representation-level leveraging cross-attention consistency technique. The figure is adapted from [64].

Rather than simply requiring coherence between 2D-3D correspondences [92], [99], [100], automatic driving algorithms demand sophisticated collaboration between in-vehicle sensors. For example, cameras and LiDAR could provide complementary information for 3D object detection promotion, such as colorful texture visualization and distance perception. Therefore, multimodal fusion is a promis-

TABLE 6
Summary of motion-based point cloud self-supervised learning pretext tasks.

Year	Method	Sub-categories	Contributions
2019	PRNet [108]	Registration	Pioneer for partial-to-partial point cloud registration enabling coarse-to-fine refinement
2021	Part mobility [109]	Registration	Converting points to trajectories to derive the rigid transformation hypotheses
2022	SuperLine3D [110]	Registration	Obtaining precise line representation under arbitrary scale perturbations
2022	DVD [111]	Registration	Learning local and global point embedding jointly
2020	PointPWC-Net [112]	Scene flow estimation	Discretizing cost volume onto 3D point clouds in a coarse-to-fine fashion
2020	Just go with the flow [113]	Scene flow estimation	Optimizing two SSL losses based on nearest neighbors and cycle consistency
2021	Self-Point-Flow [114]	Scene flow estimation	Converting pseudo label matching problem as optimal transport task

ing direction to exploit the potential of images and point clouds for acquiring complex traffic scene features.

Although not explicitly identified, Vora *et al.* [104], Wang *et al.* [105], and Li *et al.* [64] offered compact frameworks for tight sensor-fusion which could be implemented under the SSL paradigm without human annotations. PointPainting [104] was a sequential fusion method that projected LiDAR points into the semantic segmentation diagram for traffic scenes with color marking. Each point was painted with a class score obtained from the image segmentation network and then could be utilized in any LiDAR detection approach. Such painting fusion manner cleverly solved the shortcoming of depth-blurring and scale ambiguity by consolidating the bird’s-eye and camera view. PointAugmenting [105] adopted a late cross-modal fusion mechanism based on PointPainting, replacing sub-optimal segmentation scores with high-dimension CNN features containing rich outlook hints and larger receptive field to emphasize the delicate details. Moreover, a simple yet effective cross-modal data augmentation pasted virtual objects into images and point clouds guaranteeing the alignment between the camera and LiDAR. However, both PointPainting and PointAugmenting simply decorated LiDAR points with camera embedding as shown in Fig. 15(a). To improve the downstream performance, DeepFusion [64] proposed end-to-end cross-modal fusion on the feature level focusing on consistency improvement. As shown in Fig. 15(b), a block named LearnableAlign was introduced to exploit cross-attention to dynamically capture long-range correlations during the image-LiDAR fusion process to enhance the model’s recognition and localization ability.

3.4 Motion-based methods

Various point cloud frames contain rich geometric patterns and kinematic schemas that are concealed in their movement. The motion-based SSL paradigm focuses on dynamically capturing the intrinsic motion characteristics during point cloud spatial variations by taking advantage of traditional registration and scene flow estimation as pretexts. In this section, we will introduce SSL motion-based methods for point clouds with representative examples and summarize the contribution of each method in Table 6.

3.4.1 Registration

Point cloud registration is the task to merge two point clouds X and Y into a globally consistent coordinate system via estimating the rigid transformation matrix, which could be formulated as:

$$R, t = \arg \min_{R \in SO(3), t \in \mathbb{R}^3} \|\psi(RX + t) - \psi(Y)\|_2. \quad (5)$$

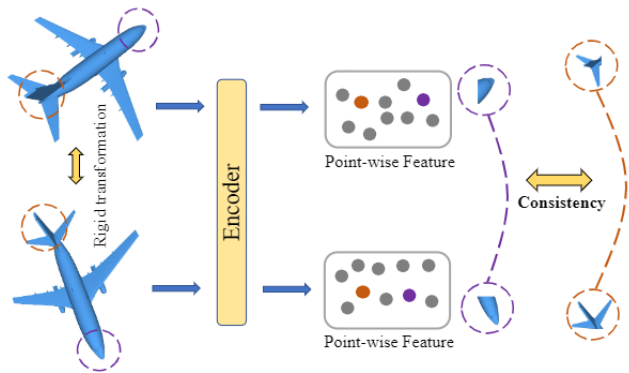


Fig. 16. The demonstration of deep versatile descriptors. The inputs are two point clouds before and after rigid transformations, where the common point components are utilized to train the encoder for global and local representation gaining. The figure is adapted from [111].

where $R \in SO(3)$ and $t \in \mathbb{R}^3$ indicates rotation matrix and translation vector, respectively. ψ is the feature extraction network learning the hierarchical informative features from dynamic point clouds. Unlike the classic ICP registration method [115] iteratively searching correspondences and estimating rigid transformation, the SSL registration paradigm can obtain the informative point cloud feature without high-quality ground-truth correspondences.

PRNet [108] was the pioneering work for partial-to-partial point cloud registration enabling coarse-to-fine refinement iteratively. Based on co-contextual information, the framework boils down the registration problem as a key point detection task, which should recognize the matching points of two input point clouds. Shi [108] presented a point cloud part mobility segmentation approach to understand the essential attributes of the dynamic object. Instead of directly processing the sequential point clouds, the raw inputs are converted to trajectories by point correspondence between successive frames to derive the rigid transformation hypotheses. Analogously, Zhao *et al.* [110] proposed an SSL line segmentation and description for LiDAR point cloud, called SuperLine3D, providing applicable line feature for global registration without any prior hints. Compared to point embedding constrained by limited resolution, this segmentation model is capable of obtaining precise line representation under arbitrary scale perturbations. Motivated by the observation that the local distinctive geometric structures of two subset point clouds are able to improve the representation expression, Liu *et al.* [111] introduced the deep versatile descriptors (DVD) regarding learning local and global point embedding jointly. As shown in Fig. 16,

the co-occurring point cloud local regions, which retain the structural knowledge under rigid transformations, are regarded as the input of DVD to extract latent geometric patterns restrained by local consistency loss. To further enhance the model’s ability of transformation awareness, reconstruction, and normal estimation are added as auxiliary tasks for better alignment.

3.4.2 Scene flow estimation

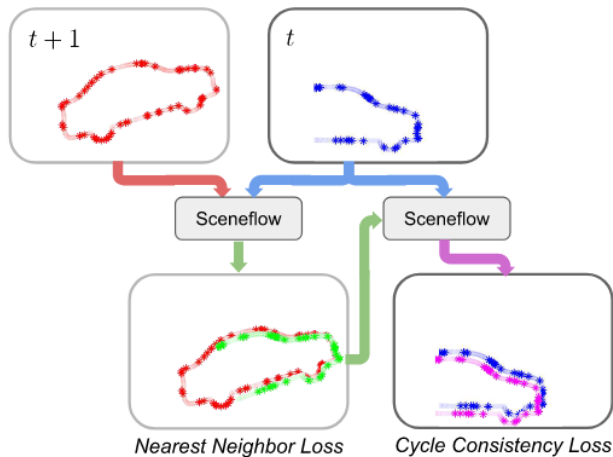


Fig. 17. The demonstration of just going with the flow. The nearest neighbor loss is utilized to push the predicted flow (green) close to the pseudo-ground truth (red) of the $t + 1$ frame. The cycle consistency loss is the penalty term to estimate the flow between predicted points (green) in the opposite direction to the original points (blue) in t frame for temporal alignment consideration. The figure is adapted from [113].

Scene flow estimation is a vital computer vision task in the point cloud field. Its objective is to estimate the motion of objects by computing dense correspondences between consecutive LiDAR scans of a scene over time. The dynamic variations of points can be represented as 3D displacement vectors to describe the motion state in terms of scene flow.

Wu *et al.* [112] were the first to introduce SSL into scene flow estimation in a learnable point-based cost volume PointPWC-Net. The cost volume is discretized as input point pair to reduce computational complexity. Additionally, an efficient upsampling strategy and wrap layers are employed to realize a coarse-to-fine fashion. Mittal *et al.* [113] proposed a novel SSL scene flow estimation network to achieve safe navigation during interactions with highly dynamic environments by optimizing two SSL losses based on nearest neighbors and cycle consistency. As shown in Fig. 17, the nearest neighbor loss encourages the points predicted based on current moment t flowing toward occupied regions of the future frame $t + 1$. The cycle consistency loss ensures that the points of the future frame $t + 1$ can be restored in the reverse direction back to frame t to avoid degenerate solutions by maintaining temporal consistency. Self-Point-Flow [114] employs more than 3D point coordinates, surface normal, and color in one-to-one matching to generate pseudo labels and concludes the pseudo label generation issue as an optimal transport problem. It leverages a random walk module to refine annotation quality by imposing local alignment.

4 DOWNSTREAM TASKS

The primary purpose of SSL is to pre-train a backbone network and transfer it to solve task-related computer vision downstream tasks. Therefore, the performance of the model in downstream tasks could reflect the effectiveness of the SSL paradigm to a certain degree. Namely, the evaluation criterion indicates whether the SSL method extracts useful implicit information from large-scale unlabeled point cloud data. In this section, we will introduce four commonly used downstream tasks as well as their respective evaluation metrics for point cloud SSL algorithm estimation. Additionally, we will summarize and compare the performance of each aforementioned SSL method in the corresponding task in a table in every subsection.

4.1 Object classification

Object classification is a fundamental and prevalent downstream task that requires the model to output a most likely category label for the given point cloud object to assess the overall semantic awareness ability of the pre-trained model. The two commonly used metrics to evaluate performance are Overall Accuracy (OA) and Mean Class Accuracy (mAcc), where the former is the ratio of correctly classified objects to the total number of objects, and the latter is the average of each class’s accuracy. Object classification can be divided into three protocols based on task settings:

- **Few-shot:** Few-shot learning (FSL) is a challenging task that involves training with limited information provided by the downstream dataset. Specifically, the n -way, m -shot setting is employed, where n is the number of classes randomly selected from the dataset and m is the number of objects randomly sampled for each class. Then, the trained model is evaluated on the test split. The few-shot protocol performance of proposed SSL methods is shown in Table 7.
- **Fine-tuning:** The SSL pre-trained feature extractor serves as the initial weights for the downstream backbone encoder, and the entire network is re-trained in a supervised manner with labels from the downstream dataset. The fine-tuning protocol performance of proposed SSL methods is presented in Table 8.
- **Linear classification:** The SSL pre-trained feature extractor is frozen by stopping the backpropagation gradient. Only a linear SVM classifier is trained in a supervised manner with downstream dataset labels. The linear classification protocol performance of proposed SSL methods is shown in Table 9.

4.2 Part segmentation

Part segmentation is a fine-grained 3D task that involves distinguishing and separating various components of an object, such as plane wings or desk legs. This task requires a model that can extract local point-level features more effectively than the overall discriminative ability required for object recognition. The evaluation criteria of point cloud part segmentation are determined by the mean Intersection over Union (mIoU), which computes the ratio of the

TABLE 7

Summary of few-shot protocol performance of proposed SSL methods on ModelNet40 [36] and ScanObjectNN [45]. The results are reported in terms of OA (%).

Method	Backbone	5-way		10-way	
		10-shot	20-shot	10-shot	20-shot
ModelNet40					
Point-MAE [54]	Transformer	96.3	97.8	92.6	95.5
Point-BERT [55]	Transformer	94.6	96.3	91.0	92.7
OcCo [60]	PointNet	89.7	92.4	89.3	89.7
OcCo [60]	DGCNN	90.6	92.5	82.9	86.5
OcCo [60]	Transformer	94.0	95.9	89.4	92.4
3D jigsaw [62]	PointNet	66.5	69.2	56.9	66.5
3D jigsaw [62]	DGCNN	34.3	42.2	26.0	29.9
MaskSurf [63]	Transformer	96.5	98.0	93.0	95.3
MaskPoint [85]	Transformer	95.0	97.2	91.4	93.4
ScanObjectNN					
Point-MAE [54]	Transformer	63.9	77.0	53.6	61.6
OcCo [60]	PointNet	70.4	72.2	54.8	61.8
OcCo [60]	DGCNN	72.4	77.2	57.0	61.6
3D jigsaw [62]	PointNet	58.6	67.6	53.6	48.1
3D jigsaw [62]	DGCNN	65.2	72.2	45.6	48.2
MaskSurf [63]	Transformer	65.3	77.4	53.8	63.2

intersection of the predicted and ground truth part labels to the union of the two, across all categories ($mIoU_C$) or all instances ($mIoU_I$). Table 1 summarizes the results of point cloud part segmentation on the ShapeNetPart dataset based on an SSL pre-training model supervised fine-tuning in terms of $mIoU_C$ (%), $mIoU_I$ (%), as well as ($mIoU$) of 16 object classes for clear demonstration and comparison.

4.3 Semantic segmentation

Similar to part segmentation, semantic segmentation requires the model to assign a semantic label to each point in the point cloud to group meaningful regions. It is frequently implemented on complicated outdoor or indoor point cloud scenes with background noise instead of a clear single object. To better compare performance, $mIoU$, OA, and $mAcc$ are commonly employed as estimation indicators to judge the feature extraction capability of pre-training models on the S3DIS dataset [41], which contains six large-scale indoor venues points in two protocols:

- **Area 5 test:** The SSL pre-trained model is fine-tuned on all areas except the largest area 5, which is chosen as the test set.
- **Six-fold cross validation:** Areas 1-6 are selected in turn as the test set and fine-tuned in the remaining 5 areas.

Both protocols of semantic segmentation performance of SSL pre-training methods are displayed in Table 11.

4.4 Object detection

Object detection is a task that involves localizing the 6 Degrees-of-Freedom (DoF) bounding box of an object and differentiating its category in a complex point cloud scene. The evaluation metric used is the average precision (AP), which measures the precision of the 3D bounding box at various recall levels. The threshold is usually set to 0.25 and 0.5. Table 12 summarizes the object detection performance of the SSL pre-training model on the SUN RGB-D [38] and ScanNet [6] datasets.

5 FUTURE DIRECTIONS

Although self-supervised learning has shown promising success in the point cloud field, we have identified current deficiencies and shortcomings in this area. We argue that SSL tasks should not be studied in isolation but rather in conjunction with advanced techniques from other domains. In this section, we will discuss possible future research directions to improve the SSL pre-training feature extraction capability and corresponding downstream performance in point clouds.

5.1 Few-shot and zero-shot learning

Generally, the dataset samples and labels used for SSL are complete and sufficient; however, such an ideal situation is difficult to achieve in real scenarios. Instead, data shortage challenges are often faced, such as damaged labels, missing information, and uneven assortment. Few-shot learning (FSL) [117] is a solution that allows the network to train under the situation of small amounts of data. This kind of technology is like a skill that a few smart people remember the emphasis only look once and can be mastered without repeated training. It is even possible to identify new sample types that have not been seen before in a test task by description alone without training samples. This amazing method is called zero-shot learning (ZSL). Both self-supervision and FSL (ZSL) [118] can free models from reliance on large annotated datasets and reduce the cost. In addition, the combination of these two can improve the generalization and understanding of the model and simulate the model’s ability to imagine the unknown.

5.2 Unified transformer-based backbone

Unlike the dominant status of CNN-based architecture in image processing, there are various networks in the point cloud field as introduced in Section 2.5. For discipline and convenience considerations, a unified architecture for point cloud feature extraction for multiple downstream tasks is needed. We believe that the transformer is a potential candidate for this purpose, where it is perfectly suitable to find the latent long-range correlations between irregular point cloud geometry. Moreover, the outstanding performance of four downstream tasks summarized in Table 7 to Table 12 employed transformers as the backbone to capture the hierarchical representation globally and locally. Therefore, we recommend adopting transformers as the unified backbone network for feature extraction in SSL point cloud research. This not only improves the performance of downstream tasks but also facilitates experimental comparisons.

5.3 Large scale 3D dataset requirement

As Section 2.3 shows, there are various 3D point cloud collections with different data structures and dense annotations that have their characteristics and provide huge support for point cloud SSL. Nevertheless, the aforementioned datasets are too homogeneous in terms of source, which is unfavorable for increasing the data diversity for domain adaptation in transfer learning. Hence, a large-scale point cloud dataset is needed that is large and varied in sample size, collects both synthetic and realistic data, and contains indoor as

TABLE 8

Summary of fine-tuning protocol performance of proposed SSL methods on ModelNet40 [36] and ScanObjectNN [45], where the input of ModelNet is 1024 and ScanObjectNN has three variant difficulty challenges. The results are reported in terms of OA (%).

Method	Year	Pretext type	Backbone	Pre-train dataset	ModelNet40	ScanObjectNN		
						OBJ-BG	OBJ-ONLY	PB-T50-RS
Supervised	2017		PointNet [10]		89.2	73.3	79.2	68.0
	2017		PointNet++ [11]		90.7	82.3	84.3	77.9
	2019	-	DGCNN [13]	-	92.9	82.8	86.2	78.1
	2017		Transformer [116]		91.4	79.86	80.55	77.24
Point-MAE [54]	2022	Reconstruction	Transformer	ShapeNet	93.8	90.02	88.29	85.18
Point-BERT [55]	2021	Reconstruction	Transformer	ShapeNet	93.2	87.43	88.12	83.07
3D jigsaw [62]	2019	Reconstruction	DGCNN	ShapeNet	92.4	82.0	82.1	-
MaskSurf [63]	2022	Reconstruction	Transformer	ShapeNet	93.40	91.22	89.17	85.81
CloudContext [69]	2019	Reconstruction	DGCNN	ShapeNet	90.8	-	-	-
UAE [72]	2022	Reconstruction	DGCNN	ShapeNet	93.2	-	-	-
MD [78]	2022	Reconstruction	DGCNN	ModelNet40	93.39	-	-	-
Self-correction [80]	2021	Reconstruction	PointNet	ShapeNet	90.0	-	-	-
Self-correction [80]	2021	Reconstruction	RSCNN	ShapeNet	93.0	-	-	-
MaskPoint [85]	2022	Reconstruction	Transformer	ShapeNet	93.8	88.1	89.3	84.3
Info3D [86]	2020	Contrast	PointNet	ShapeNet	90.20	-	-	-
Info3D [86]	2020	Contrast	DGCNN	ShapeNet	93.03	-	-	-
OcCo [60]	2021	Alignment	PointNet	ModelNet40	90.1	-	-	-
OcCo [60]	2021	Alignment	DGCNN	ModelNet40	93.0	82.1	83.2	-
Cross-view [99]	2021	Alignment	DGCNN	ModelNet40	93.0	82.2	83.0	-
Multi-view rendering [100]	2022	Alignment	PointNet	ModelNet40	89.5	78.5	80.5	-
Multi-view rendering [100]	2022	Alignment	DGCNN	ModelNet40	93.2	84.5	84.3	-
STRL [102]	2021	Alignment	DGCNN	ShapeNet	93.1	-	-	-

TABLE 9

Summary of linear classification protocol performance of proposed SSL methods on ModelNet10/40 [36]. The results are reported in terms of OA (%).

Method	Pretext type	Backbone	ModelNet10/40
Point-MAE [54]	Reconstruction	Transformer	- / 91.41
Orientation estimation [61]	Reconstruction	PointNet	- / 88.6
Orientation estimation [61]	Reconstruction	DGCNN	- / 90.75
3D jigsaw [62]	Reconstruction	PointNet	91.61 / 87.31
3D jigsaw [62]	Reconstruction	DGCNN	94.52 / 90.64
MaskSurf [63]	Reconstruction	Transformer	- / 92.26
CloudContext [69]	Reconstruction	DGCNN	94.5 / 89.3
UAE [72]	Reconstruction	DGCNN	95.6 / 92.9
Pose Disentanglement [76]	Reconstruction	PointNet	- / 90.1
Pose Disentanglement [76]	Reconstruction	DGCNN	- / 92.0
CP-Net [77]	Reconstruction	RSCNN	- / 91.9
FoldingNet [79]	Reconstruction	GNN	94.4 / 88.4
Self-correction [80]	Reconstruction	PointNet	93.3 / 89.9
Self-correction [80]	Reconstruction	RSCNN	95.0 / 92.4
PC-GAN [82]	Reconstruction	GAN	- / 87.5
Info3D [86]	Contrast	PointNet	- / 89.8
Info3D [86]	Contrast	DGCNN	- / 91.6
AFSRL [87]	Contrast	GNN	- / 91.5
Contrasting and clustering [88]	Contrast	DGCNN	93.8 / 86.8
Hard negatives [89]	Contrast	DGCNN	- / 89.6
OcCo [60]	Alignment	DGCNN	- / 89.2
Cross-view [99]	Alignment	GNN	- / 89.8
Multi-view rendering [100]	Alignment	PointNet	- / 89.7
Multi-view rendering [100]	Alignment	DGCNN	- / 91.7
STRL [102]	Alignment	PointNet	- / 88.3
STRL [102]	Alignment	DGCNN	- / 90.9
PRNet [108]	Motion	DGCNN	- / 85.2

well as outdoor scenes. We believe such a comprehensive dataset will be of great help for the development of point cloud SSL to further enhance the model’s generalizability and robustness.

5.4 Various modalities interactions

Despite the assorted modalities gathered in outdoor autonomous driving datasets [35], [48], [49] by different sensors, researchers normally focus on the point cloud data

TABLE 10

Summary of part segmentation performance of proposed SSL methods on ShapeNetPart [41].

Method	Type	Backbone	mIoU _C	mIoU _I
Supervised		PointNet [10]	83.39	83.7
		PointNet++ [11]	81.85	85.1
		DGCNN [13]	82.33	85.2
		Transformer [116]	83.42	85.1
Point-MAE [54]	Reconstruction	Transformer	84.19	86.1
Point-BERT [55]	Reconstruction	Transformer	84.11	85.6
3D jigsaw [62]	Reconstruction	PointNet	-	82.2
3D jigsaw [62]	Reconstruction	DGCNN	-	85.3
MaskSurf [63]	Reconstruction	Transformer	84.36	86.1
CloudContext [69]	Reconstruction	DGCNN	-	81.5
UAE [72]	Reconstruction	DGCNN	-	85.6
Pose Disentanglement [76]	Reconstruction	PointNet	- / 83.8	-
Pose Disentanglement [76]	Reconstruction	DGCNN	- / 85.1	-
MD [78]	Reconstruction	DGCNN	-	85.5
Self-correction [80]	Reconstruction	PointNet	-	84.1
Self-correction [80]	Reconstruction	RSCNN	-	85.2
MaskPoint [85]	Reconstruction	Transformer	84.4	86.0
AFSRL [87]	Contrast	GNN	- / 85.7	-
Hard negatives [89]	Contrast	DGCNN	- / 82.3	-
PointContrast [90]	Contrast	U-Net	-	85.1
OcCo [60]	Alignment	PointNet	-	83.4
OcCo [60]	Alignment	DGCNN	-	85.0
Cross-view [99]	Alignment	DGCNN	79.1	83.7
Multi-view rendering [100]	Alignment	PointNet	-	83.3
Multi-view rendering [100]	Alignment	DGCNN	-	84.7
PRNet [108]	Motion	DGCNN	78.8 / 82.5	-

only while ignoring the connections and alignment relationships between them. This approach cannot fulfill the potential of such multimodal collections. With the rapid development of multimodal models [64], [104], [105], we believe that a storm of cross-modal SSL point cloud paradigm is coming. This paradigm will fuse diverse modalities (e.g., natural language, radar, voice) more than images to maximize the unique perspectives of each modality to complement each other while highlighting repetitions for validation.

TABLE 11
Summary of semantic segmentation performance of proposed SSL methods on S3DIS [41].

Method	Type	Backbone	OA	mAcc	mIoU
Supervised	-	PointNet [10]	78.6	49.0	47.7
		DGCNN [13]	84.1	-	56.1
		Transformer [116]	86.8	68.6	60.0
Area 5 test					
Point-MAE [54]	Reconstruction	Transformer	87.4	69.4	61.0
OcCo [60]	Alignment	PointNet	-	83.6	44.5
OcCo [60]	Alignment	DGCNN	-	87.0	49.5
3D jigsaw [62]	Reconstruction	PointNet	-	82.5	43.6
3D jigsaw [62]	Reconstruction	DGCNN	-	86.8	48.2
MaskSurf [63]	Reconstruction	Transformer	88.3	69.9	61.6
PointContrast [90]	Contrast	SR-UNet	-	77.0	70.9
Contrastive Scene Contexts [91]	Contrast	DGCNN	-	-	73.8
DepthContrast [94]	Contrast	PointNet++	-	72.1	64.8
Multi-view rendering [100]	Alignment	PointNet	-	85.0	46.7
Multi-view rendering [100]	Alignment	DGCNN	-	87.0	49.9
Six-fold cross validation					
OcCo [60]	Alignment	PointNet	82.0	-	54.9
OcCo [60]	Alignment	DGCNN	84.6	-	58.0
3D jigsaw [62]	Reconstruction	PointNet	80.1	-	52.6
3D jigsaw [62]	Reconstruction	DGCNN	84.1	-	55.6
CloudContext [69]	Reconstruction	DGCNN	78.9	-	47.6
Multi-view rendering [100]	Alignment	PointNet	-	83.2	52.1
Multi-view rendering [100]	Alignment	DGCNN	-	87.5	59.0

TABLE 12
Summary of object detection performance of proposed SSL methods on SUN RGB-D [38] and ScanNet [6]. The pre-training input only contains the point cloud geometry.

Method	Type	Backbone	SUN RGB-D		ScanNet	
			AP ₂₅	AP ₅₀	AP ₂₅	AP ₅₀
Point-BERT [55]	Reconstruction	Transformer	-	-	61.0	38.3
MaskPoint [85]	Reconstruction	Transformer	-	-	64.2	42.0
PointContrast [90]	Contrast	SR-UNet	57.5	34.8	59.2	38.0
PointContrast [90]	Contrast	VoteNet	59.2	38.0	57.5	34.8
DepthConst [94]	Contrast	PointNet++	-	-	61.3	-
DepthConst [94]	Contrast	VoteNet	64.0	42.9	61.6	35.5
DepthConst [94]	Contrast	H3DNet	69.0	50.0	63.5	43.4
Multi-view rendering [100]	Alignment	DGCNN	58.1	35.1	60.3	39.2
STRL [102]	Alignment	VoteNet	58.2	-	-	-

5.5 Hierarchical feature extraction

To cope with sophisticated and varied downstream tasks requiring overall semantic understanding (e.g., object classification) as well as fine-grained geometrical awareness (e.g., part segmentation), the SSL pre-training model should have the ability of global perception and local analysis. Particularly, the interactions between hierarchical levels need to be regarded to discover the implicit relation in terms of disorder permutations. Therefore, we suggest that hierarchical feature extraction should be embedded in the forthcoming SSL paradigm to improve the model’s ability to capture the global and local information of point clouds.

5.6 Multiple tasks pre-training

Up to now, most point cloud SSL schemas have only one specific pre-training pretext while few works train diverse tasks concurrently such as BERT [16]. The main resistance is that multi-tasking has to consider the compatibility and synergy between various pretexts simultaneously and distribute fitting weights to each loss item for steady parameter updating. Indeed, distinct proxies could provide multi-level information from various perspectives of point clouds so that jointly training multiple tasks could facilitate the network to learn more comprehensive representations from all sides.

5.7 Theory and interpretability

Similar to traditional deep learning, point cloud SSL has the same shortcomings that lack theoretical support and poor

interpretation. The process of model training is a black-box operation, making it difficult for researchers to analyze the results, which could only be implemented by an ablation study alternatively. Most of the paradigms are improved based on previous work by drawing empirical conclusions. Such ‘tried and tested’ research methods miss rigorous proof and are therefore challenging to generalize and replicate. We suggest that future studies should include an inquiry into explainable theory. For example, well-established theories from mutual information [119] or causal inference [120] can be applied in the structure of the network and the design of the loss function. Such a theoretical and explainable paradigm would be more generalizable and robust.

6 CONCLUSION

Point cloud self-supervised learning fundamentally moves away from a model’s reliance on manual annotation via the design of pre-training pretext tasks to enable the network to extract effective information from raw data and achieve exciting progress competitive to supervised learning in various downstream computer vision tasks. This paper extensively outlines recent representative deep neural network-based methods for self-supervised learning in the point cloud from a comprehensive perspective, including the background introduction, dataset collections, data augmentation summary, etc. A novel taxonomy is proposed to systematically classify the current point cloud SSL pretext tasks into four general categories demonstrated by a detailed explanation as well as performance comparison. Finally, future research directions are discussed to provide a broad and insightful view of the current state-of-the-art methods in point cloud SSL. We hope this paper can provide a comprehensive overview of the current point cloud SSL research and inspire more researchers to explore the potential of this promising paradigm.

7 ACKNOWLEDGEMENT

This work received financial support from Jiangsu Industrial Technology Research Institute (JITRI) and Wuxi National Hi-Tech District (WND).

REFERENCES

- [1] N. El-Sheimy and Y. Li, “Indoor navigation: State of the art and future trends,” *Satellite Navigation*, vol. 2, no. 1, pp. 1–23, 2021.
- [2] Y. Li, L. Ma, Z. Zhong, F. Liu, D. Cao, J. Li, and M. A. Chapman, “Deep learning for lidar point clouds in autonomous driving: A review,” *IEEE Transactions on Neural Networks*, 2020.
- [3] Z. Yang, S. Liu, H. Hu, L. Wang, and S. Lin, “Reppoints: Point set representation for object detection,” in *Proceedings of the IEEE/CVF international conference on computer vision*, 2019, pp. 9657–9666.
- [4] D. Matti, H. K. Ekenel, and J.-P. Thiran, “Combining lidar space clustering and convolutional neural networks for pedestrian detection,” in *2017 14th IEEE International Conference on Advanced Video and Signal Based Surveillance (AVSS)*, 2017, pp. 1–6.
- [5] B. Wu, X. Zhou, S. Zhao, X. Yue, and K. Keutzer, “SqueezeSegV2: Improved model structure and unsupervised domain adaptation for road-object segmentation from a lidar point cloud,” in *2019 International Conference on Robotics and Automation (ICRA)*. IEEE, 2019, pp. 4376–4382.
- [6] A. Dai, A. X. Chang, M. Savva, M. Halber, T. Funkhouser, and M. Nießner, “ScanNet: Richly-annotated 3d reconstructions of indoor scenes,” in *Proceedings of the IEEE conference on computer vision and pattern recognition*, 2017, pp. 5828–5839.

- [7] M. B. Sariyildiz, Y. Kalantidis, K. Alahari, and D. Larlus, "Improving the generalization of supervised models," *arXiv preprint arXiv:2206.15369*, 2022.
- [8] G. Csurka, "Domain adaptation for visual applications: A comprehensive survey," *arXiv preprint arXiv:1702.05374*, 2017.
- [9] Y. Zhang, J. Lin, R. Li, K. Jia, and L. Zhang, "Point-dae: Denoising autoencoders for self-supervised point cloud learning," *arXiv preprint arXiv:2211.06841*, 2022.
- [10] C. R. Qi, H. Su, K. Mo, and L. J. Guibas, "Pointnet: Deep learning on point sets for 3d classification and segmentation," in *Proceedings of the IEEE conference on computer vision and pattern recognition*, 2017, pp. 652–660.
- [11] C. R. Qi, L. Yi, H. Su, and L. J. Guibas, "Pointnet++: Deep hierarchical feature learning on point sets in a metric space," *Advances in neural information processing systems*, vol. 30, 2017.
- [12] Y. Zhou and O. Tuzel, "Voxelnet: End-to-end learning for point cloud based 3d object detection," *computer vision and pattern recognition*, 2018.
- [13] Y. Wang, Y. Sun, Z. Liu, S. E. Sarma, M. M. Bronstein, and J. M. Solomon, "Dynamic graph cnn for learning on point clouds," *Acm Transactions On Graphics (tog)*, vol. 38, no. 5, pp. 1–12, 2019.
- [14] A. Xiao, J. Huang, D. Guan, and S. Lu, "Unsupervised representation learning for point clouds: A survey," *arXiv preprint arXiv:2202.13589*, 2022.
- [15] T. Mikolov, K. Chen, G. Corrado, and J. Dean, "Efficient estimation of word representations in vector space," *arXiv preprint arXiv:1301.3781*, 2013.
- [16] J. Devlin, M.-W. Chang, K. Lee, and K. Toutanova, "Bert: Pre-training of deep bidirectional transformers for language understanding," *arXiv preprint arXiv:1810.04805*, 2018.
- [17] L. Floridi and M. Chiriatti, "Gpt-3: Its nature, scope, limits, and consequences," *Minds and Machines*, vol. 30, pp. 681–694, 2020.
- [18] M. Lewis, Y. Liu, N. Goyal, M. Ghazvininejad, A. Mohamed, O. Levy, V. Stoyanov, and L. Zettlemoyer, "Bart: Denoising sequence-to-sequence pre-training for natural language generation, translation, and comprehension," *arXiv preprint arXiv:1910.13461*, 2019.
- [19] C. Doersch, A. Gupta, and A. A. Efros, "Unsupervised visual representation learning by context prediction," in *Proceedings of the IEEE international conference on computer vision*, 2015, pp. 1422–1430.
- [20] M. Noroozi and P. Favaro, "Unsupervised learning of visual representations by solving jigsaw puzzles," in *European conference on computer vision*. Springer, 2016, pp. 69–84.
- [21] S. Gidaris, P. Singh, and N. Komodakis, "Unsupervised representation learning by predicting image rotations," *international conference on learning representations*, 2018.
- [22] D. Pathak, P. Krähenbühl, J. Donahue, T. Darrell, and A. A. Efros, "Context encoders: Feature learning by inpainting," *computer vision and pattern recognition*, 2016.
- [23] K. He, X. Chen, S. Xie, Y. Li, P. Dollár, and R. Girshick, "Masked autoencoders are scalable vision learners," *arXiv preprint arXiv:2111.06377*, 2021.
- [24] T. Chen, S. Kornblith, M. Norouzi, and G. Hinton, "A simple framework for contrastive learning of visual representations," in *International conference on machine learning*. PMLR, 2020, pp. 1597–1607.
- [25] K. He, H. Fan, Y. Wu, S. Xie, and R. Girshick, "Momentum contrast for unsupervised visual representation learning," in *Proceedings of the IEEE/CVF conference on computer vision and pattern recognition*, 2020, pp. 9729–9738.
- [26] M. Caron, I. Misra, J. Mairal, P. Goyal, P. Bojanowski, and A. Joulin, "Unsupervised learning of visual features by contrasting cluster assignments," *Advances in Neural Information Processing Systems*, vol. 33, pp. 9912–9924, 2020.
- [27] A. Faktor and M. Irani, "Video segmentation by non-local consensus voting," in *BMVC*, vol. 2, no. 7, 2014, p. 8.
- [28] O. Stretcu and M. Leordeanu, "Multiple frames matching for object discovery in video," in *BMVC*, vol. 1, no. 2, 2015, p. 3.
- [29] I. Croitoru, S.-V. Bogolin, and M. Leordeanu, "Unsupervised learning from video to detect foreground objects in single images," in *Proceedings of the IEEE International Conference on Computer Vision*, 2017, pp. 4335–4343.
- [30] H. Jiang, G. Larsson, M. M. G. Shakhnarovich, and E. Learned-Miller, "Self-supervised relative depth learning for urban scene understanding," in *Proceedings of the European Conference on Computer Vision (ECCV)*, 2018, pp. 19–35.
- [31] R. Arandjelovic and A. Zisserman, "Look, listen and learn," in *Proceedings of the IEEE international conference on computer vision*, 2017, pp. 609–617.
- [32] P. Agrawal, J. Carreira, and J. Malik, "Learning to see by moving," in *Proceedings of the IEEE international conference on computer vision*, 2015, pp. 37–45.
- [33] D. Jayaraman and K. Grauman, "Learning image representations tied to ego-motion," in *Proceedings of the IEEE International Conference on Computer Vision*, 2015, pp. 1413–1421.
- [34] L. Jing and Y. Tian, "Self-supervised visual feature learning with deep neural networks: A survey," *IEEE transactions on pattern analysis and machine intelligence*, vol. 43, no. 11, pp. 4037–4058, 2020.
- [35] A. Geiger, P. Lenz, and R. Urtasun, "Are we ready for autonomous driving? the kitti vision benchmark suite," in *2012 IEEE conference on computer vision and pattern recognition*. IEEE, 2012, pp. 3354–3361.
- [36] Z. Wu, S. Song, A. Khosla, F. Yu, L. Zhang, X. Tang, and J. Xiao, "3d shapenets: A deep representation for volumetric shapes," in *Proceedings of the IEEE conference on computer vision and pattern recognition*, 2015, pp. 1912–1920.
- [37] A. X. Chang, T. Funkhouser, L. Guibas, P. Hanrahan, Q. Huang, Z. Li, S. Savarese, M. Savva, S. Song, H. Su *et al.*, "Shapenet: An information-rich 3d model repository," *arXiv preprint arXiv:1512.03012*, 2015.
- [38] S. Song, S. P. Lichtenberg, and J. Xiao, "Sun rgb-d: A rgb-d scene understanding benchmark suite," in *Proceedings of the IEEE conference on computer vision and pattern recognition*, 2015, pp. 567–576.
- [39] B.-S. Hua, Q.-H. Pham, D. T. Nguyen, M.-K. Tran, L.-F. Yu, and S.-K. Yeung, "Scenenn: A scene meshes dataset with annotations," in *2016 fourth international conference on 3D vision (3DV)*. Ieee, 2016, pp. 92–101.
- [40] Y. Xiang, W. Kim, W. Chen, J. Ji, C. Choy, H. Su, R. Mottaghi, L. Guibas, and S. Savarese, "Objectnet3d: A large scale database for 3d object recognition," in *European conference on computer vision*. Springer, 2016, pp. 160–176.
- [41] I. Armeni, O. Sener, A. R. Zamir, H. Jiang, I. Brilakis, M. Fischer, and S. Savarese, "3d semantic parsing of large-scale indoor spaces," in *Proceedings of the IEEE conference on computer vision and pattern recognition*, 2016, pp. 1534–1543.
- [42] T. Hackel, N. Savinov, L. Ladicky, J. D. Wegner, K. Schindler, and M. Pollefeys, "Semantic3d. net: A new large-scale point cloud classification benchmark," *arXiv preprint arXiv:1704.03847*, 2017.
- [43] X. Sun, J. Wu, X. Zhang, Z. Zhang, C. Zhang, T. Xue, J. B. Tenenbaum, and W. T. Freeman, "Pix3d: Dataset and methods for single-image 3d shape modeling," in *Proceedings of the IEEE conference on computer vision and pattern recognition*, 2018, pp. 2974–2983.
- [44] S. Koch, A. Matveev, Z. Jiang, F. Williams, A. Artemov, E. Burnaev, M. Alexa, D. Zorin, and D. Panozzo, "Abc: A big cad model dataset for geometric deep learning," in *Proceedings of the IEEE/CVF Conference on Computer Vision and Pattern Recognition*, 2019, pp. 9601–9611.
- [45] M. A. Uy, Q.-H. Pham, B.-S. Hua, T. Nguyen, and S.-K. Yeung, "Revisiting point cloud classification: A new benchmark dataset and classification model on real-world data," in *Proceedings of the IEEE/CVF international conference on computer vision*, 2019, pp. 1588–1597.
- [46] K. Mo, S. Zhu, A. X. Chang, L. Yi, S. Tripathi, L. J. Guibas, and H. Su, "Partnet: A large-scale benchmark for fine-grained and hierarchical part-level 3d object understanding," in *Proceedings of the IEEE/CVF conference on computer vision and pattern recognition*, 2019, pp. 909–918.
- [47] S. A. Taghanaki, J. Luo, R. Zhang, Y. Wang, P. K. Jayaraman, and K. M. Jatavallabhula, "Robustpointset: A dataset for benchmarking robustness of point cloud classifiers," *arXiv preprint arXiv:2011.11572*, 2020.
- [48] P. Sun, H. Kretzschmar, X. Dotiwalla, A. Chouard, V. Patnaik, P. Tsui, J. Guo, Y. Zhou, Y. Chai, B. Caine *et al.*, "Scalability in perception for autonomous driving: Waymo open dataset," in *Proceedings of the IEEE/CVF conference on computer vision and pattern recognition*, 2020, pp. 2446–2454.
- [49] H. Caesar, V. Bankiti, A. H. Lang, S. Vora, V. E. Liong, Q. Xu, A. Krishnan, Y. Pan, G. Baldan, and O. Beijbom, "nusenes: A multimodal dataset for autonomous driving," in *Proceedings of*

- the IEEE/CVF conference on computer vision and pattern recognition, 2020, pp. 11 621–11 631.
- [50] Q. Hu, B. Yang, S. Khalid, W. Xiao, N. Trigoni, and A. Markham, "Towards semantic segmentation of urban-scale 3d point clouds: A dataset, benchmarks and challenges," in *Proceedings of the IEEE/CVF conference on computer vision and pattern recognition*, 2021, pp. 4977–4987.
- [51] M. Chen, Q. Hu, T. Hugues, A. Feng, Y. Hou, K. McCullough, and L. Soibelman, "Stpls3d: A large-scale synthetic and real aerial photogrammetry 3d point cloud dataset," *arXiv preprint arXiv:2203.09065*, 2022.
- [52] G. A. Miller, "Wordnet: a lexical database for english," *Communications of the ACM*, vol. 38, no. 11, pp. 39–41, 1995.
- [53] M. Everingham, L. Van Gool, C. K. I. Williams, J. Winn, and A. Zisserman, "The PASCAL Visual Object Classes Challenge 2012 (VOC2012) Results," <http://www.pascal-network.org/challenges/VOC/voc2012/workshop/index.html>.
- [54] Y. Pang, W. Wang, F. E. Tay, W. Liu, Y. Tian, and L. Yuan, "Masked autoencoders for point cloud self-supervised learning," *arXiv preprint arXiv:2203.06604*, 2022.
- [55] X. Yu, L. Tang, Y. Rao, T. Huang, J. Zhou, and J. Lu, "Pointbert: Pre-training 3d point cloud transformers with masked point modeling," *arXiv preprint arXiv:2111.14819*, 2021.
- [56] A. R. Zamir, A. Sax, W. Shen, L. J. Guibas, J. Malik, and S. Savarese, "Taskonomy: Disentangling task transfer learning," in *Proceedings of the IEEE conference on computer vision and pattern recognition*, 2018, pp. 3712–3722.
- [57] D. A. S. Fraser, "Probability and statistics: Theory and applications," Tech. Rep., 1976.
- [58] M.-H. Guo, J.-X. Cai, Z.-N. Liu, T.-J. Mu, R. R. Martin, and S.-M. Hu, "Pct: Point cloud transformer," *Computational Visual Media*, vol. 7, no. 2, pp. 187–199, 2021.
- [59] I. Goodfellow, J. Pouget-Abadie, M. Mirza, B. Xu, D. Warde-Farley, S. Ozair, A. Courville, and Y. Bengio, "Generative adversarial nets," *Advances in neural information processing systems*, vol. 27, 2014.
- [60] H. Wang, Q. Liu, X. Yue, J. Lasenby, and M. J. Kusner, "Unsupervised point cloud pre-training via occlusion completion," in *Proceedings of the IEEE/CVF international conference on computer vision*, 2021, pp. 9782–9792.
- [61] O. Poursaeed, T. Jiang, H. Qiao, N. Xu, and V. G. Kim, "Self-supervised learning of point clouds via orientation estimation," in *2020 International Conference on 3D Vision (3DV)*. IEEE, 2020, pp. 1018–1028.
- [62] J. Sauder and B. Sievers, "Self-supervised deep learning on point clouds by reconstructing space," *Advances in Neural Information Processing Systems*, vol. 32, 2019.
- [63] Y. Zhang, J. Lin, C. He, Y. Chen, K. Jia, and L. Zhang, "Masked surfel prediction for self-supervised point cloud learning," *arXiv preprint arXiv:2207.03111*, 2022.
- [64] Y. Li, A. W. Yu, T. Meng, B. Caine, J. Ngiam, D. Peng, J. Shen, Y. Lu, D. Zhou, Q. V. Le *et al.*, "Deepfusion: Lidar-camera deep fusion for multi-modal 3d object detection," in *Proceedings of the IEEE/CVF Conference on Computer Vision and Pattern Recognition*, 2022, pp. 17 182–17 191.
- [65] C. Min, D. Zhao, L. Xiao, Y. Nie, and B. Dai, "Voxel-mae: Masked autoencoders for pre-training large-scale point clouds," *arXiv preprint arXiv:2206.09900*, 2022.
- [66] G. Hess, J. Jaxing, E. Svensson, D. Hagerman, C. Petersson, and L. Svensson, "Masked autoencoders for self-supervised learning on automotive point clouds," *arXiv preprint arXiv:2207.00531*, 2022.
- [67] M. Afham, I. Dissanayake, D. Dissanayake, A. Dharmasiri, K. Thilakarathna, and R. Rodrigo, "Crosspoint: Self-supervised cross-modal contrastive learning for 3d point cloud understanding," in *Proceedings of the IEEE/CVF Conference on Computer Vision and Pattern Recognition*, 2022, pp. 9902–9912.
- [68] Z. Wu, Y. Xiong, S. X. Yu, and D. Lin, "Unsupervised feature learning via non-parametric instance discrimination," in *Proceedings of the IEEE conference on computer vision and pattern recognition*, 2018, pp. 3733–3742.
- [69] J. Sauder and B. Sievers, "Context prediction for unsupervised deep learning on point clouds," *arXiv preprint arXiv:1901.08396*, vol. 2, no. 4, p. 5, 2019.
- [70] R. Li, X. Li, C.-W. Fu, D. Cohen-Or, and P.-A. Heng, "Pu-gan: a point cloud upsampling adversarial network," in *Proceedings of the IEEE/CVF international conference on computer vision*, 2019, pp. 7203–7212.
- [71] Y. Zhao, L. Hui, and J. Xie, "Sspu-net: Self-supervised point cloud upsampling via differentiable rendering," in *Proceedings of the 29th ACM International Conference on Multimedia*, 2021, pp. 2214–2223.
- [72] C. Zhang, J. Shi, X. Deng, and Z. Wu, "Upsampling autoencoder for self-supervised point cloud learning," *arXiv preprint arXiv:2203.10768*, 2022.
- [73] X. Liu, X. Liu, Y.-S. Liu, and Z. Han, "Spu-net: Self-supervised point cloud upsampling by coarse-to-fine reconstruction with self-projection optimization," *IEEE Transactions on Image Processing*, vol. 31, pp. 4213–4226, 2022.
- [74] H. Liu, H. Yuan, J. Hou, R. Hamzaoui, and W. Gao, "Pufa-gan: A frequency-aware generative adversarial network for 3d point cloud upsampling," *IEEE Transactions on Image Processing*, vol. 31, pp. 7389–7402, 2022.
- [75] W. Zhao, X. Liu, Z. Zhong, J. Jiang, W. Gao, G. Li, and X. Ji, "Self-supervised arbitrary-scale point clouds upsampling via implicit neural representation," in *Proceedings of the IEEE/CVF Conference on Computer Vision and Pattern Recognition*, 2022, pp. 1999–2007.
- [76] M.-S. Tsai, P.-Z. Chiang, Y.-H. Tsai, and W.-C. Chiu, "Self-supervised feature learning from partial point clouds via pose disentanglement," in *2022 IEEE/RSJ International Conference on Intelligent Robots and Systems (IROS)*. IEEE, 2022, pp. 1031–1038.
- [77] M. Xu, Z. Zhou, H. Xu, Y. Wang, and Y. Qiao, "Cp-net: Contour-perturbed reconstruction network for self-supervised point cloud learning," *arXiv preprint arXiv:2201.08215*, 2022.
- [78] C. Sun, Z. Zheng, X. Wang, M. Xu, and Y. Yang, "Self-supervised point cloud representation learning via separating mixed shapes," *IEEE Transactions on Multimedia*, 2022.
- [79] Y. Yang, C. Feng, Y. Shen, and D. Tian, "Foldingnet: Point cloud auto-encoder via deep grid deformation," in *Proceedings of the IEEE conference on computer vision and pattern recognition*, 2018, pp. 206–215.
- [80] Y. Chen, J. Liu, B. Ni, H. Wang, J. Yang, N. Liu, T. Li, and Q. Tian, "Shape self-correction for unsupervised point cloud understanding," in *Proceedings of the IEEE/CVF International Conference on Computer Vision*, 2021, pp. 8382–8391.
- [81] I. Achituve, H. Maron, and G. Chechik, "Self-supervised learning for domain adaptation on point clouds," in *Proceedings of the IEEE/CVF Winter Conference on Applications of Computer Vision*, 2021, pp. 123–133.
- [82] C.-L. Li, M. Zaheer, Y. Zhang, B. Poczoz, and R. Salakhutdinov, "Point cloud gan," *arXiv preprint arXiv:1810.05795*, 2018.
- [83] M. Sarmad, H. J. Lee, and Y. M. Kim, "Rl-gan-net: A reinforcement learning agent controlled gan network for real-time point cloud shape completion," in *Proceedings of the IEEE/CVF Conference on Computer Vision and Pattern Recognition*, 2019, pp. 5898–5907.
- [84] D. W. Shu, S. W. Park, and J. Kwon, "3d point cloud generative adversarial network based on tree structured graph convolutions," in *Proceedings of the IEEE/CVF international conference on computer vision*, 2019, pp. 3859–3868.
- [85] H. Liu, M. Cai, and Y. J. Lee, "Masked discrimination for self-supervised learning on point clouds," *arXiv preprint arXiv:2203.11183*, 2022.
- [86] A. Sanghi, "Info3d: Representation learning on 3d objects using mutual information maximization and contrastive learning," in *European Conference on Computer Vision*. Springer, 2020, pp. 626–642.
- [87] Z. Lu, Y. Dai, W. Li, and Z. Su, "Joint data and feature augmentation for self-supervised representation learning on point clouds," *arXiv preprint arXiv:2211.01184*, 2022.
- [88] L. Zhang and Z. Zhu, "Unsupervised feature learning for point cloud understanding by contrasting and clustering using graph convolutional neural networks," in *2019 international conference on 3D vision (3DV)*. IEEE, 2019, pp. 395–404.
- [89] B. Du, X. Gao, W. Hu, and X. Li, "Self-contrastive learning with hard negative sampling for self-supervised point cloud learning," in *Proceedings of the 29th ACM International Conference on Multimedia*, 2021, pp. 3133–3142.
- [90] S. Xie, J. Gu, D. Guo, C. R. Qi, L. Guibas, and O. Litany, "Pointcontrast: Unsupervised pre-training for 3d point cloud understanding," in *European conference on computer vision*. Springer, 2020, pp. 574–591.

- [91] J. Hou, B. Graham, M. Nießner, and S. Xie, "Exploring data-efficient 3d scene understanding with contrastive scene contexts," in *Proceedings of the IEEE/CVF Conference on Computer Vision and Pattern Recognition*, 2021, pp. 15 587–15 597.
- [92] S. Lal, M. Prabhudesai, I. Mediratta, A. W. Harley, and K. Fragkiadaki, "Coconets: Continuous contrastive 3d scene representations," in *Proceedings of the IEEE/CVF Conference on Computer Vision and Pattern Recognition*, 2021, pp. 12 487–12 496.
- [93] Y. Liu, L. Yi, S. Zhang, Q. Fan, T. Funkhouser, and H. Dong, "P4Contrast: Contrastive Learning with Pairs of Point-Pixel Pairs for RGB-D Scene Understanding," *arXiv e-prints*, p. arXiv:2012.13089, Dec. 2020.
- [94] Z. Zhang, R. Girdhar, A. Joulin, and I. Misra, "Self-supervised pretraining of 3d features on any point-cloud," in *Proceedings of the IEEE/CVF International Conference on Computer Vision*, 2021, pp. 10 252–10 263.
- [95] A. v. d. Oord, Y. Li, and O. Vinyals, "Representation learning with contrastive predictive coding," *arXiv preprint arXiv:1807.03748*, 2018.
- [96] P. Velickovic, W. Fedus, W. L. Hamilton, P. Liò, Y. Bengio, and R. D. Hjelm, "Deep graph infomax." *ICLR (Poster)*, vol. 2, no. 3, p. 4, 2019.
- [97] S. Xie, S. Liu, Z. Chen, and Z. Tu, "Attentional shapecontextnet for point cloud recognition," in *Proceedings of the IEEE conference on computer vision and pattern recognition*, 2018, pp. 4606–4615.
- [98] J. Yang, J. M. Alvarez, and M. Liu, "Self-supervised learning of depth inference for multi-view stereo," in *Proceedings of the IEEE/CVF Conference on Computer Vision and Pattern Recognition*, 2021, pp. 7526–7534.
- [99] L. Jing, L. Zhang, and Y. Tian, "Self-supervised feature learning by cross-modality and cross-view correspondences," in *Proceedings of the IEEE/CVF Conference on Computer Vision and Pattern Recognition*, 2021, pp. 1581–1591.
- [100] B. Tran, B.-S. Hua, A. T. Tran, and M. Hoai, "Self-supervised learning with multi-view rendering for 3d point cloud analysis," in *Proceedings of the Asian Conference on Computer Vision*, 2022, pp. 3086–3103.
- [101] H. Wang, L. Yang, X. Rong, J. Feng, and Y. Tian, "Self-supervised 4d spatio-temporal feature learning via order prediction of sequential point cloud clips," in *Proceedings of the IEEE/CVF Winter Conference on Applications of Computer Vision*, 2021, pp. 3762–3771.
- [102] S. Huang, Y. Xie, S.-C. Zhu, and Y. Zhu, "Spatio-temporal self-supervised representation learning for 3d point clouds," in *Proceedings of the IEEE/CVF International Conference on Computer Vision*, 2021, pp. 6535–6545.
- [103] B. Mersch, X. Chen, J. Behley, and C. Stachniss, "Self-supervised point cloud prediction using 3d spatio-temporal convolutional networks," in *Conference on Robot Learning*. PMLR, 2022, pp. 1444–1454.
- [104] S. Vora, A. H. Lang, B. Helou, and O. Beijbom, "Pointpainting: Sequential fusion for 3d object detection," in *Proceedings of the IEEE/CVF conference on computer vision and pattern recognition*, 2020, pp. 4604–4612.
- [105] C. Wang, C. Ma, M. Zhu, and X. Yang, "Pointaugmenting: Cross-modal augmentation for 3d object detection," in *Proceedings of the IEEE/CVF Conference on Computer Vision and Pattern Recognition*, 2021, pp. 11 794–11 803.
- [106] D. Xu, J. Xiao, Z. Zhao, J. Shao, D. Xie, and Y. Zhuang, "Self-supervised spatiotemporal learning via video clip order prediction," in *Proceedings of the IEEE/CVF Conference on Computer Vision and Pattern Recognition*, 2019, pp. 10 334–10 343.
- [107] J.-B. Grill, F. Strub, F. Altché, C. Tallec, P. Richemond, E. Buchatskaya, C. Doersch, B. Avila Pires, Z. Guo, M. Gheshlaghi Azar *et al.*, "Bootstrap your own latent—a new approach to self-supervised learning," *Advances in Neural Information Processing Systems*, vol. 33, pp. 21 271–21 284, 2020.
- [108] Y. Wang and J. M. Solomon, "Prnet: Self-supervised learning for partial-to-partial registration," *Advances in neural information processing systems*, vol. 32, 2019.
- [109] Y. Shi, X. Cao, and B. Zhou, "Self-supervised learning of part mobility from point cloud sequence," in *Computer Graphics Forum*, vol. 40, no. 6. Wiley Online Library, 2021, pp. 104–116.
- [110] X. Zhao, S. Yang, T. Huang, J. Chen, T. Ma, M. Li, and Y. Liu, "Superline3d: Self-supervised line segmentation and description for lidar point cloud," in *Computer Vision—ECCV 2022: 17th European Conference, Tel Aviv, Israel, October 23–27, 2022, Proceedings, Part IX*. Springer, 2022, pp. 263–279.
- [111] D. Liu, C. Chen, C. Xu, R. Qiu, and L. Chu, "Self-supervised point cloud registration with deep versatile descriptors," *arXiv preprint arXiv:2201.10034*, 2022.
- [112] W. Wu, Z. Y. Wang, Z. Li, W. Liu, and L. Fuxin, "Pointpwc-net: Cost volume on point clouds for (self-) supervised scene flow estimation," in *European conference on computer vision*. Springer, 2020, pp. 88–107.
- [113] H. Mittal, B. Okorn, and D. Held, "Just go with the flow: Self-supervised scene flow estimation," in *Proceedings of the IEEE/CVF conference on computer vision and pattern recognition*, 2020, pp. 11 177–11 185.
- [114] R. Li, G. Lin, and L. Xie, "Self-point-flow: Self-supervised scene flow estimation from point clouds with optimal transport and random walk," in *Proceedings of the IEEE/CVF conference on computer vision and pattern recognition*, 2021, pp. 15 577–15 586.
- [115] P. J. Besl and N. D. McKay, "Method for registration of 3-d shapes," in *Sensor fusion IV: control paradigms and data structures*, vol. 1611. Spie, 1992, pp. 586–606.
- [116] A. Vaswani, N. Shazeer, N. Parmar, J. Uszkoreit, L. Jones, A. N. Gomez, Ł. Kaiser, and I. Polosukhin, "Attention is all you need," *Advances in neural information processing systems*, vol. 30, 2017.
- [117] V. Garcia and J. Bruna, "Few-shot learning with graph neural networks," *arXiv preprint arXiv:1711.04043*, 2017.
- [118] B. Romera-Paredes and P. Torr, "An embarrassingly simple approach to zero-shot learning," in *International conference on machine learning*. PMLR, 2015, pp. 2152–2161.
- [119] N. Sayed, B. Brattoli, and B. Ommer, "Cross and learn: Cross-modal self-supervision," in *German Conference on Pattern Recognition*. Springer, 2018, pp. 228–243.
- [120] W. Wang, X. Lin, F. Feng, X. He, M. Lin, and T.-S. Chua, "Causal representation learning for out-of-distribution recommendation," in *Proceedings of the ACM Web Conference 2022*, 2022, pp. 3562–3571.